BEST POSSIBLE SCAN

BRL

REPORT NO. 1155
DECEMBER 1961

EFFECTS OF METEOROID IMPACTS ON SPACE VEHICLES

R. J. Eichelberger
J. W. Gehring

NOX

Department of the Army Project No. 503-04-011
Ordnance Management Structure Code No. 5010.11.833

BALLISTIC RESEARCH LABORATORIES

ABERDEEN PROVING GROUND, MARYLAND

BALLISTIC RESEARCH LABORATORIES

REPORT NO. 1155

DECEMBER 1961

EFFECTS OF METEOROID IMPACTS ON SPACE VEHICLES

R. J. Eichelberger
J. W. Gehring

Terminal Ballistics Laboratory

Department of the Army Project No. 503-04-011
Ordnance Management Structure Code No. 5010.11.833

ABERDEEN PROVING GROUND, MARYLAND

BALLISTIC RESEARCH LABORATORIES

REPORT NO. 1155

RJEichelberger/JWGehring/ic
Aberdeen Proving Ground, Md.
December 1961

EFFECTS OF METEOROID IMPACTS ON SPACE VEHICLES*

ABSTRACT

The mechanism of crater formation due to hypervelocity impact is described, using a variety of experimental observations and theory as a basis. The currently accepted empirical correlations are also presented. The evidence is considered in the light of the problem of meteoroid impacts upon space vehicles, and such generalized predictions as are possible at the present state of the art are derived.

*Presented at the American Rocket Society, Space Flight Report to the Nation, New York Coliseum, October 9-15, 1961.

I. INTRODUCTION

The purpose of the present paper is not to present a chart or graph showing the precise thicknesses of various materials required to provide adequate protection against puncture by meteoroids, nor to give estimates of rate of erosion due to repeated impacts by smaller bodies. The literature is already replete with such information, the various estimates often being in disagreement by several orders of magnitude[1]. The authors' purpose is to present as clear and complete (but non-mathematical) a description of the mechanism of crater formation in hypervelocity impact as is possible at the present state of the art, together with such data and empirical relationships as have been well established. Much of the information available has been obtained under experimental conditions not even remotely simulating those of meteoroids striking the relatively thin skin of a space vehicle, so that some effort will be made to expose the basic principles involved and to demonstrate the similarity, in principle, of the laboratory observations to the effects that will be encountered in space vehicles.

II. DEBRIS IN SPACE

There have been numerous estimates of the frequency of encounter, the mass distribution, and the physical properties of meteoroids, based on various types of observation and conjecture.[2] Figure 1 shows one opinion (no preference for this particular estimate is implied) which illustrates the range of conditions that must be considered. On the whole, only particles in the micron size range and having masses less than 10^{-4} grams are likely to be encountered with any significant frequency. Consequently, the space vehicle problem corresponds more to hypervelocity crater formation in thick targets than to perforation of thin plates. The meteoroid velocity range is fairly well defined; essentially all meteoroids are expected to have velocities between 11 and 70 km/sec. Impact velocities, of course, can be greater or less by an amount equal to the velocity of the vehicle, so the range of impact velocities may be from practically zero to greater than 80 km/sec.

Opinion as to the density and other physical properties of the meteorites varies widely but, as will be shown, this is of little consequence.

III. LABORATORY SIMULATION AND OBSERVATION TECHNIQUES

The techniques for projection of "hypervelocity" particles and of observing the effects of impact have been considerably improved and their range of capabilities increased in the past two years. In the investigations whose results are described here, explosive projection techniques have been used exclusively. A number of different devices with different characteristics provide projectiles with a wide range of both velocities and masses, as shown in Table I. The range of conditions that can be attained by further development, using proven principles and techniques are shown, in addition to the ranges covered by past and current experiments. The variations in mass cover the entire range of primary concern in space travel, and the velocities extend well into the lower portion of the range of interest, but capabilities still fall considerably short of the upper portion of the velocity range. However, as will be demonstrated, the higher velocities currently attainable are sufficiently high to assure that the mechanisms of crater formation being observed are typical of the high velocity regime; furthermore, the relationships developed are valid over a sufficiently wide range of conditions as to lend a considerable degree of confidence to extrapolations into the higher portion of the velocity range.

Consistent with the purpose of studying the fundamental aspects of the problem, instrumentation has been diverse and elaborate. High speed photography has been used for sub-microsecond observations of surface phenomena and, in transparent target materials, such interior processes as crater expansion, shock propagation, and fracture.[3] Flash X-ray photography has been used to observe both surface and interior behavior, including measurements of transient density changes.[3] Several new techniques have been developed which permit measurement of particle velocity[4] and of pressure-time profiles[5] during crater formation. Use has also been made of more mundane techniques such as impulse measurement by ballistic pendulum and recovery of spall and fragment residue, in order to assure a complete quantitative analysis.

IV. CRATER FORMATION - FUNDAMENTAL OBSERVATIONS

The manner in which a crater forms after an impact at high velocity is best illustrated by flash radiography. In Figure 2 is shown a series of pictures, taken with an exposure time of 0.2 μsec. at the time intervals indicated after impact by a steel pellet upon an aluminum target. The pellet's mass was 0.18 gm. and its velocity 5.0 km/sec. The progressive growth of the crater over a period of approximately 30 to 35 μsec. can be readily seen; careful inspection of the last picture shows that the dimensions of the crater have actually decreased due to elastic (and possibly some plastic) recovery. During the very early stages, the remnants of the impacting body can be discerned at the bottom of the growing crater, but in the later pictures (i.e. after 5 μsec.) it has completely disappeared except for some small fragments deposited on the walls of the crater. Although the pictures are difficult to reproduce, a shell of highly compressed target material adjacent to the crater surface can be detected in several cases.

Another important aspect of crater formation is illustrated in Figure 3. The pictures represent a sequence of flash radiographs taken at the indicated time intervals after impacts on lead targets; they show the front (impacted) surfaces and are intended to demonstrate the manner and extent of ejection of target material from the crater. The material flows along the surface of the expanding crater and is ejected at moderately high velocities. At high impact velocities, the mass of material ejected in this manner is very considerable; the total momentun in the "backward" direction associated with this "back-splash" is many times greater than the initial momentum (in the forward direction) of the impacting body, so that the total forward momentum that must somehow be absorbed by the target body is also many times greater than that of the projectile.[6] The implications are of critical importance in space vehicle protection, as will be shown later. The extraordinarily long time required to complete crater formation in materials like lead, even at modest impact velocities, is also evident in Figure 3.

Some of the details of crater formation are better illustrated by using transparent targets and optical photography. Figure 4 is a series of framing camera pictures, taken at a rate of 0.5 million frames per second, showing the effects of an impact on Lucite. In the early frames, the pellet can be seen approaching the target; the apparent termination of its ionization trail is due to the edge of the Fresnel lens used for back-lighting. In the first few frames after impact, the expanding crater can be seen, but no detached shock wave ahead of it; in the third frame after impact, the shock wave is finally seen to detach itself and thereafter the crater and the shock wave expand at different velocities. After about seven frames, the crater ceases to increase in dimensions, but the shock wave continues, gradually degrading into an elastic wave.

For quantitative purposes, a streak camera provides better data than a framing camera. A rotating mirror camera picture of an impact similar to that represented in Figure 4 is shown in Figure 5; it constitutes a time-distance plot of events occurring in a plane that contains the trajectory of the impacting pellet, and shows the pellet (1), the shock wave in the target (2), the surface of the expanding crater (3), and the envelope of cracks propagating through the target (4). More complicated, special techniques have been developed to obtain the same data for opaque materials.

Representative data showing results obtained by the various techniques are shown in Figures 6 and 7. Figure 6 shows the intensity of the shock wave in Lucite as a function of distance from the impact point, for an impact at a velocity of 4.6 km/sec. The initial pressure is determined by the shock properties of the pellet and target materials and the impact velocity; it corresponds to the theoretical prediction for a plane impact. The pressure falls off very rapidly, however, as the wave propagates into the material, even during the period in which the crater expands so rapidly that the shock wave cannot detach. This is consistent with the concept that, as soon as deformation of projectile and target begins, the pressure at the contact surface will fall to the Bernoulli value (for compressible materials). The magnitudes of the pressures should be particularly noted, together with the fact that the pressure, for a given pair of materials, will increase as the square of

the impact velocity. Thus, for a steel projectile striking Lucite at a velocity of 46 km/sec. (10 times that of the test) an initial pressure of 33 megabars (about 5×10^8 psi) would be expected. The same conditions would be produced by a meteoroid having properties similar to those of Lucite striking steel at 46 km/sec.

The rates of crater expansion in Lucite, aluminum, and lead are shown in Figures 6 and 7. It will be particularly noted that the crater in Lucite is complete in a much shorter time than in aluminum, after impacts by similar projectiles, even though the projectile is "used up" more quickly in aluminum. In lead, the crater continues to expand for a much longer time, even after impact at a much lower velocity.

The experimental evidence cited is intended only for illustration. It is further supported by electronic measurements of pressure, measurements of particle velocity, and measurements of density. The interpretation of the data has, in nearly all cases been checked by using two or more methods of observation. Observations have been made over a wide range of velocities (3 km/sec to 20 km/sec) and of projectile masses (10^{-11} to 10 grams) and materials to assure that the behaviour described is generally representative. The results of all of the experimental observations have been synthesized into a physical model of the phenomenon.

V. MODEL OF CRATER FORMATION

The model that has evolved from the combined theoretical and experimental studies to date is illustrated schematically by Figure 8. The projectile approaches the target initially at a velocity considerably in excess of wave propagation velocity in either material. Immediately after contact, a transient state is entered in which the pressure at the interface is that pertaining to a plane impact without flow - i.e. in the megabar range. Shock waves propagate a short distance from the contact surface into both the projectile and the target and at the same time release of pressure at the boundary of the projectile initiates lateral flow of both materials. As a result, in a very small fraction of a microsecond, an equilibrium condition is set up in which the two shock waves become stationary with respect to the projectile-target interface. During this steady-state regime, which also persists for only a fraction of a microsecond, the hydrodynamic theory that has been formulated for

shaped charges[7] can be applied; it is particularly important in considering perforation of thin sheets because the projectile is progressively "used up", as illustrated in the third and fourth stages of Figure 8. It is characteristic of truly hypervelocity impact that the rate of crater expansion during this second stage is greater than the wave propagation velocities in the target material; consequently, the region of compressed material is confined to a thin shell adjacent to the crater surface and the energy density is extremely high.

After the impacting body has been completely deformed and removed as a causative force from the system, the shock wave continues to expand and the crater with it; the intensity and velocity of the shock decrease; but the crater surface undergoes a more rapid decrease in velocity so that the shock wave detaches itself and the thickness of the shell of compressed target material increases. This stage continues until the energy density behind the shock wave becomes too small to overcome the intrinsic resistance to deformation of the material, at which point the shock wave continues to expand as a low-intensity plastic or elastic wave; the crater then may shrink somewhat due to plastic and elastic recovery. In brittle materials the tensile stresses produced by reflection of the shock wave from free surfaces will produce fracture and spall that may, in extreme cases, obscure the form of the original crater entirely.

During the second and third stages of crater formation, the deformation is mainly shear parallel to the walls of the expanding crater. The flow velocity is very high so that the projectile material and the target material are both ejected from the crater with considerable velocity. It is only at relatively low velocities that the pellet material is found plated or scattered as small particles over the surface of the final crater. The amount of shear occurring at extremely high strain rates is responsible for the classification of target materials in two groups; ductile and frangible. The ductile materials, including all metals as well as waxes, wet clay, etc., flow for a much longer time after impact, apparently because of a decrease in their resistance to deformation at extreme strain rates. This behaviour is not clearly understood, but is similar to that used in some new impact extrusion processes. The frangible materials include the long chain polymers, siliceous materials, and stones; they have in common, in addition to their brittleness, a monotonic increase in resistance to deformation with increasing strain rate, even at the very

high rates involved in hypervelocity impact. As a result, the crater stops expanding in Lucite earlier than in aluminum (see Figures 6 and 7) despite the relative magnitudes of their static shear strengths.

This peculiarity of ductile materials has been one of the main sources of difficulty in formulating a complete theory. Hydrodynamic calculations[8] yield accurate detailed predictions for the initial stages of the process, but fail to correctly predict final crater dimensions because they take no account of the "after flow" of the target material. Since a very large fraction of the crater expansion takes place during this stage, the result is a complete disagreement between calculations and experiment as to depth of penetration and crater volume, or the variations in crater dimensions with change in velocity.

During the initial stages of the process, some fusion and ionization of both projectile material and target material occur[9]. However, neither phenomenon has any detectable effect upon the correlations obtained.

Reviewing the model described above it is readily evident that different properties of impacting and impacted bodies are of importance during the various stages of crater formation. In the first, transient stage, the impact velocity and the Hugoniot properties are the only important ones in establishing the pressures. The lateral dimensions, relative to length of the projectile will determine the length of time required to achieve the equilibrium condition that is typical of the following stage; if the length is only a small fraction of the smallest lateral dimension, the steady-state regime will be unimportant - the energy will be dissipated during the transient regime and a broad, shallow crater will be obtained instead of the classical hemisphere.

In the second, steady-state stage, the densities and compressibilities of the projectile and target materials are of importance, as well as the velocity and the dimensions of the projectile; all enter into an evaluation of the intensity and the duration of the pressure pulse produced during this stage. The duration of the steady-state regime can be estimated roughly to be

$$(1) \qquad t = \frac{L}{V} \left(1 + \sqrt{\rho_P/\rho_T} \right)$$

where L is the length of the projectile, V the impact velocity, ρ_p the density of the projectile, and ρ_T the density of the target. Both compressibility and strength are neglected in this simple formula, but it provides useful orders of magnitude. For example, a meteorite 1 mm in length striking a body of equal density at a velocity of 40 km/sec. would produce a steady-state regime lasting only 0.05 μ sec and would penetrate a distance of 1 mm into the body during that time. The duration of the preceding transient regime would have been much shorter, however. For projectiles whose length is many times greater than their lateral dimensions, the steady-state stage of the process becomes far more significant and the crater formation becomes very similar to a shaped charge jet penetration[7].

The theoretical aspects of the third, "cavitation", stage are more obscure. In principle, it would be expected that the profile of the pressure wave developed during the first two stages would be of some importance, as well as the strength of the impacted body. In practice, as will be shown below, only the resistance of the target material is of measurable significance. This stage of the process becomes so dominant in high speed impacts on ductile materials that the effects of the density and compressibility of the target material and of the density, compressibility, and even the dimensions of the projectile cannot be detected in empirical correlations. Returning to the example in the preceding paragraph, if the target body were sufficiently thick, the final crater would be a hemisphere about 12 mm deep in 2S0 aluminum or about 6.4 mm deep in 75ST alloy. Thus, the craters would be 12 mm deep by 22 mm in diameter in the 2S0 and 6.4 mm deep by 10.8 mm in diameter in the 75ST targets - so nearly hemispherical that only careful measurement would distinguish the difference. In the experiments represented by Figures 6 and 7, the durations of the two chief stages of crater formation and the depths of the crater at the end of each would be, approximately:

Target	Duration (μ sec)		Crater Depth (mm)	
	Steady-state	Cavitation	Steady-state	Cavitation
Lucite (V=5 km/sec)	0.7	8	2.5	15
2S0 Aluminum (V= 5 km/sec)	0.5	40	1.7	12
Lead (V=2.4 km/sec)	0.8	100	0.8	24

Even at modest impact velocities, the craters will appear to be very nearly hemispherical, if the pressure at the contact surface is sufficient to freely deform the projectile.

The extent of the final recovery and shrinkage depends entirely upon the mechanical properties of the target material. Little work has been done on this stage.

The final conclusion from all of the theoretical and basic experimental work is that for "reasonable" shapes of bodies impacting at meteoroid velocities on metallic targets, hemispherical craters will be produced, the dimensions of which will be, to a good approximation, independent of all properties of the target except its resistance to shear deformation. For the so-called frangible target materials, the detailed properties of the projectile and the target are more likely to be important and empirical correlations may reflect a mixture of momentum-dependent and energy-dependent phenomena.

Some qualitative predictions relevant to impact against thin layers can also be drawn from the model described. First, the impacting body itself will not penetrate a layer thicker than, roughly,

$$T = L \sqrt{\rho_P / \rho_T} \qquad (2)$$

although a perforation will be produced in thicknesses many times greater, and spall from the target layer will be projected behind. Second, in ductile materials, because of the major contribution of cavitation to the crater dimensions, and the relatively long time required for the flow to take place, the diameter of the hole produced in a thin plate should be considerably less than the diameter of the crater in a thick plate; the hole diameter should decrease systematically with decreasing plate thickness because the stress required to support continued flow will be relieved by shock reflection in a thin plate before

the process is completed. This will not be as important, however, in the case of frangible materials. Thirdly, if the layer is thin enough to permit penetration by the meteoroid itself, reflection of shocks set up by the impact will probably result in shattering and dispersion of the meteoroid, although porous bodies are sometimes compacted instead. Fourth, the spall ejected from the rear surface of the plate will generally be dispersed over a fairly large solid angle. This effect, added to the probable shattering of the meteoroid itself, comprise the basis of the "Whipple bumper" concept for protection of space vehicles. A word of caution must be sounded regarding dependence upon this device, however. Momentum considerations applied to the above model for impact at very high velocities suggest that the concentration of spall particles together with the multiplication of momentum may result in greater rather than less damage to components behind.

Some conjecture concerning the effect of oblique incidence can also be drawn from the model. At high impact velocities, the length of time required to transfer all of the energy from the projectile to the target is so short compared to the total time of crater formation that the problem can be treated, to a fairly good approximation, as one of instantaneous deposition of energy on a small area. Consequently, the craters would be expected to remain hemispherical even at large angles of incidence. Momentum considerations, however, indicate that the "cratering efficiency" should decrease with increasing obliquity of incidence, although no thorough theoretical analysis of the problem has been carried out.

The model outlined mainly represents a synthesis of the basic experimental observations made at the Ballistic Research Laboratories. It is, however, in close agreement with those portions of the current theoretical treatments that are valid; the latter are still undergoing refinement at the BRL and elsewhere. The model is also in close aggreement with empirical correlations that have been obtained, in general. In some specific cases apparent disagreements can be found, but they are without exception the results of observations at relatively low velocities; in all such cases known to the authors, a careful inspection of trends

observed when impact velocity is increased indicates that the model is entirely valid for the conditions of interest in the meteoroid problem. No attempt will be made here to describe the mathematical theory in detail, but a representative sampling of empirical correlations is presented in the next section.

VI. EMPIRICAL CORRELATION

The data presented in the following pertain exclusively to the "ductile" target materials. Corresponding observations with frangible materials are not available because of the difficulty of obtaining usable measurements of the dimensions of the true crater; as noted earlier, the effects of profuse fracture and spallation often totally obscure the form of the crater.

A. Crater Shape

It has previously been established in the literature[10] that craters produced by hypervelocity impact are typically hemispherical. The craters shown in Figure 9 have often been used to illustrate the progressive approach to the hemispherical shape as impact velocity is increased. Actually, the crater is only approximately hemispherical, since the steady-state penetration contributes a cylindrical section near the target surface. Careful measurements[11] have shown that the depth of the crater is given very accurately by the formula

$$(3) \quad P = \frac{D}{2} + T$$

where D is the diameter and T is given by equation (2).

B. Volume-Energy

The linear relation between the volume of the crater resulting from hypervelocity impact has been established previously[10]. Figure 10 is presented here, nonetheless, because it demonstrates the range of validity of the correlation. It is clear that the linear correlation holds very well for a wide variety of target materials. Furthermore the data used in Figure 10 (each point represents the mean of a number of observations) cover a range of particle masses from 10^{-11} to 10 grams, illustrating the range of proven validity of the established scaling laws[11]. While the velocity range covered in Figure 10 barely reaches

the lower boundary of the meteoroid velocity range, it does extend beyond experimental data published previously. Data obtained at the BRL with the short jet devices are not included because the masses are not as precisely determined, at present, as for the other projection devices; however, the available observations lie well within the uncertainty in mass determination of the regression lines of Figure 10, extrapolated to velocities up to 21 km/sec, indicating that the linear relationship can be used with a fair degree of confidence throughout the meteoroid velocity range.

C. Target Strength

In discussing the model of crater formation, the importance of resistance to shear deformation at high strain rates as a controlling parameter was emphasized. In practice, the large variations in mechanical properties of nominally identical target materials have necessitated the use of a gauge of resistance that can be measured directly on individual targets. For this purpose, the Brinell hardness has been found to provide a surprisingly good criterion[11][12]. In Figure 11 is shown a correlation between the ratio of kinetic energy of the impacting body to volume of crater produced and the Brinell hardness number. It should be emphasized that the data represent results from a number of sources, obtained with projectiles ranging in mass from 10^{-11} to 10 gm. and in velocity to 15 km/sec; furthermore, pellets of a variety of shapes and of materials ranging from nylon to tungsten carbide have been used. The points lying farthest from the correlation line, without exception, represent the cases in which the target strengths were least well known (handbook values have been used in some cases), and invariably repetition of experiments using targets of known hardness has yielded closer agreement. The results support very strongly the conclusion from fundamental considerations that cavitation plays the dominant role in crater formation in ductile materials and explains the linear relationship between volume and energy.

D. Temperature Effects

The effect of changing target temperature has been investigated for a number of materials. Typical results are illustrated in Figure 12. The variations in crater volume with temperature are entirely consistent with the changes in metallurgical properties of the materials (specifically, the shear strength) even to the apparently peculiar behaviour of copper, 17SO aluminum alloy, and zinc[13]. Thus, the data simply reinforce the conclusions concerning the role of resistance to deformation.

E. Anisotropic Effects

Still further support is found from tests with microparticles fired against single crystal targets and against targets in which the grain size is of the same order as that of the impacting body[14]. In all such experiments, asymmetric craters have been observed, as illustrated in Figure 13 the shape depending in an entirely predictable manner upon the degree of anisotropy of the crystal and its orientation.

F. Oblique Impact

The effect of oblique incidence of the impacting body upon crater formation is of considerable interest in the space vehicle problem. It has been shown that, at moderate impact velocities, the craters remain essentially hemispherical until an angle is reached at which the component of projectile velocity normal to the target surface falls below the sound velocity in the target material. While this is only a rough "rule-of-thumb", without theoretical basis at present, it serves as a useful criterion for all the materials tested. The crater behaviour upon oblique impact is illustrated by the flash radiographs in Figure 14 and by the sectioned targets in Figure 15. In the meteoroid problem, only impacts at very large angles of obliquity would yield other than hemispherical craters.

The dimensions of the craters vary with angle of incidence regardless of the shape of the crater, as illustrated by the plot in Figure 16[15]. The effect is great enough to be of considerable importance in estimating damage to a space vehicle. Only a rudimentary theoretical explanation of this effect is available at present.

G. Thin Targets

While the vast majority of meteoroids will be of such small size that their effect on a space vehicle would fall in the category of crater formation in a thick target or, in the aggregate, as surface erosion by cratering, there will be occasional ones large enough to perforate an outer layer of any reasonable thickness. In these cases, the size of the hole produced and the nature of damage done behind the first layer may be of crucial importance.

In Figure 17 is shown a typical set of observations on the variation in hole diameter with plate thickness for constant impact conditions[16]. The diameter increases systematically from a value only slightly greater than the diameter of the projectile, for very thin sheets, to the diameter of a crater in an infinite target. This is entirely in accord with predictions from the model. Figure 18 shows a pair of plots of the mass of material, both remnants of the projectile and spall from the target, and Figure 19 shows the spatial distribution of material behind a target plate for two typical cases. Unfortunately, these data cannot be taken as typical of meteoroid impacts; the impact velocities were too low to assure the free deformation of the impacting body, as illustrated by Figure 20. However, the results are in such close agreement with predictions from the model of crater formation for impacts at appropriate velocities as to encourage some degree of confidence in the predictions for meteoroid impacts.

VII. CONCLUSIONS

The model of crater formation presented in Section V is supported by such a variety and mass of experimental evidence, as well as theoretical reasoning, as to appear beyond serious question, at least in its qualitative features. There remains a great deal of experimental work on crater formation itself and on the behaviour of materials at very high strain rates, in addition to the subsequent refinement of theory,

before a complete mathematical description of the phenomenon can be expected. Nonetheless, with the model as a guide and with the available experimental data as a foundation, predictions pertaining to a wide range of conditions can be made with considerable confidence.

On the other hand, one of the very weak points in the current state of knowledge is the lack of information on perforation of thin targets at meteoroid velocities. The word of caution concerning dependence upon "bumpers" for protection of space vehicles must be repeated. Model considerations indicate that the concentration and damaging capacity of spall behind a thin plate will increase very rapidly at higher impact velocities. Observations at moderate velocities support this expectation. Only direct experimental test, using techniques that are now available, but have not yet been exploited for this purpose, will provide the critically needed quantitative data.

Considering the present state of uncertainty concerning the physical properties of meteoroids, and the tremendous range of vehicle design possible, the authors do not deem it appropriate to present plots of predicted damage. Instead, the following "rules of thumb" are submitted for use by the reader:

1. In sufficiently thick skins, a meteoroid having kinetic energy E, (in a coordinate system fixed with respect to the space vehicle), will produce a hemispherical crater of volume τ, given by

$$(4) \quad \tau = 4 \times 10^{-9} \frac{E}{B} \quad \text{(c.g.s. units)}$$

where B is the Brinell hardness number of the skin material.

2. If the thickness of the skin is less than $(\frac{3\tau}{2})^{1/3}$ (or even if it is slightly greater), the skin will be perforated.

3. No remnant of the impacting body will penetrate a thickness greater then T given by equation (2) without severe reduction in velocity. Using these rules, one can make up his own estimates of damage for any preferred type of meteoroid or vehicle design.

R. J. EICHELBERGER J. W. GEHRING

REFERENCES

1. Beard, David B., "Meteoric Impact," Jour. of ARS, Vol. 31, No. 1, January 1961; also Whipple, F.L., "The Meteoric Risk to Space Vehicles," Vistas In Astronautics, Pergamon Press, New York, 1958; and Rodriquez, David, "Meteoroid Shielding For Space Vehicles," Aerospace Engineering, Vol. 19, No. 12, Dec. 1960.

2. Jonah, F. C., "Critical Analysis of Solid Debris In Space," IAS Paper No. 60-73, 1960, and Martin, H. L., "The Meteoroid Hazard To Space Travel," ABMA Report No. DV-TN-22-59, 5 Aug. 1959.

3. Gehring, J. W., Jr., "High Speed Radiographic and Optical Techniques Applied to Hypervelocity Impact Studies," Proceedings of the 5th International Congress on High Speed Photography, SMPTE, Washington, D.C., Oct. 1961.

4. Unpublished work of Robert Franz, BRL, APG, Md.

5. Eichelberger, R. J., and Hauver, G. E., "Solid State Transducers For Recording of Intense Pressure Pulses," Colloques Internationaux Du Centre National De Ta Recherche Scientifique, Paris, 28 August - 2 Sept. 1961, and Hauver G. E., "Characteristics of Several Dilectric Materials At High Pressures," BRL Tech. Note No. 1356, Oct. 1960.

6. Stanyukovick, K. P., "Concerning The Impact of Solids At High Velocities," Jour. of Exptl. and Theor. Phys., (U.S.S.R.), 36, 1605-1606, May 1959.

7. Eichelberger, R. J., "Experimental Test of the Theory of Penetration By Metallic Jets," Jour. of App. Phys., Vol. 27, No. 1, 63-68, Jan. 1956.

8. Bjork, R. L., "Effects of a Meteoroid Impact On Steel and Aluminum In Space," Tech. Report p-1662, Rand Corporation, Engineering Division, Dec 16, 1958.

9. Bartlett, R. W., Cook, M.A., and Keyes, R. T., "Observations of Vaporization Accompanying Ultra-High Velocity Impact," University of Utah, Air Force Office of Scientific Research, AFOSR-TN-60-327, 4 Jan. 1960.

10. Eichelberger, R. J., Allison, F. E. and Donaldson, W. F., "Craters Formed By High-Velocity Fragments," Fundamentals of Shaped Charges, Carnegie Inst. of Tech., Contract No. DA-36-061-ORD-394, July 1954, Chapter I.

11. Proceedings of the Third Symposium On Hypervelocity Impact, Armor Research Foundation, Chicago, Ill., 7-9 October 1959, see for instance papers by J. H. Kineke, F. L. Culp, J. W. Gehring, and others.

12. Feldman, J. B., Jr., "Volume-Energy Relation From Shaped Charge Jet Penetrations," Proc. of the 4th Symp. on Hypervelocity Impact, Eglin AFB, Fla., Apr. 26-28, 1960, APGC-TR-60-39.

13. Allison, F. E., Becker, K. R., and Vitali, R., "Effects of Target Temperature On Hypervelocity Cratering," Proc. of 4th Symp. on Hypervelocity Impact, Eglin AFB, Fla., Apr. 26-28, 1960, APGC-TR-60-39. Work supported under contract with the BRL, APG, Md.

14. Gehring, J. W. and Richards, L. G., "Further Studies of Microparticle Cratering In A Variety of Target Materials," Proc. of 4th Symp. on Hypervelocity Impact, Eglin AFB, Fla., Apr. 26-28, 1960, APGC-TR-60-39.

15. Bryan, G. M., " A Model of Oblique Impact," Proc. of 4th Symp on Hypervelocity Impact, Eglin AFB, Fla., Apr. 26-28, 1960, APGC-TR-60-39. Work supported under contract with the BRL, APG, Md.

16. Watson, R., Carnegie Inst. of Tech., Pittsburgh, Pa., work supported under contract to BRL, APG, Md., to be published.

METEOR SIMULATION AT THE BRL

	Current		Potential	
	Mass (gm)	Velocity (km/sec)	Mass (gm)	Velocity (km/sec)
Micro Particles	10^{-11} to 10^{-5}	8 to 15	10^{-12} to 10^{-4}	7 to > 20
Simple Shapes	10^{-2} to 10	0 to 7	10^{-2} to 100	0 to 8
Short Jets	10^{-1} to 10	8 to 20	10^{-2} to 100	7 to 30

TABLE I

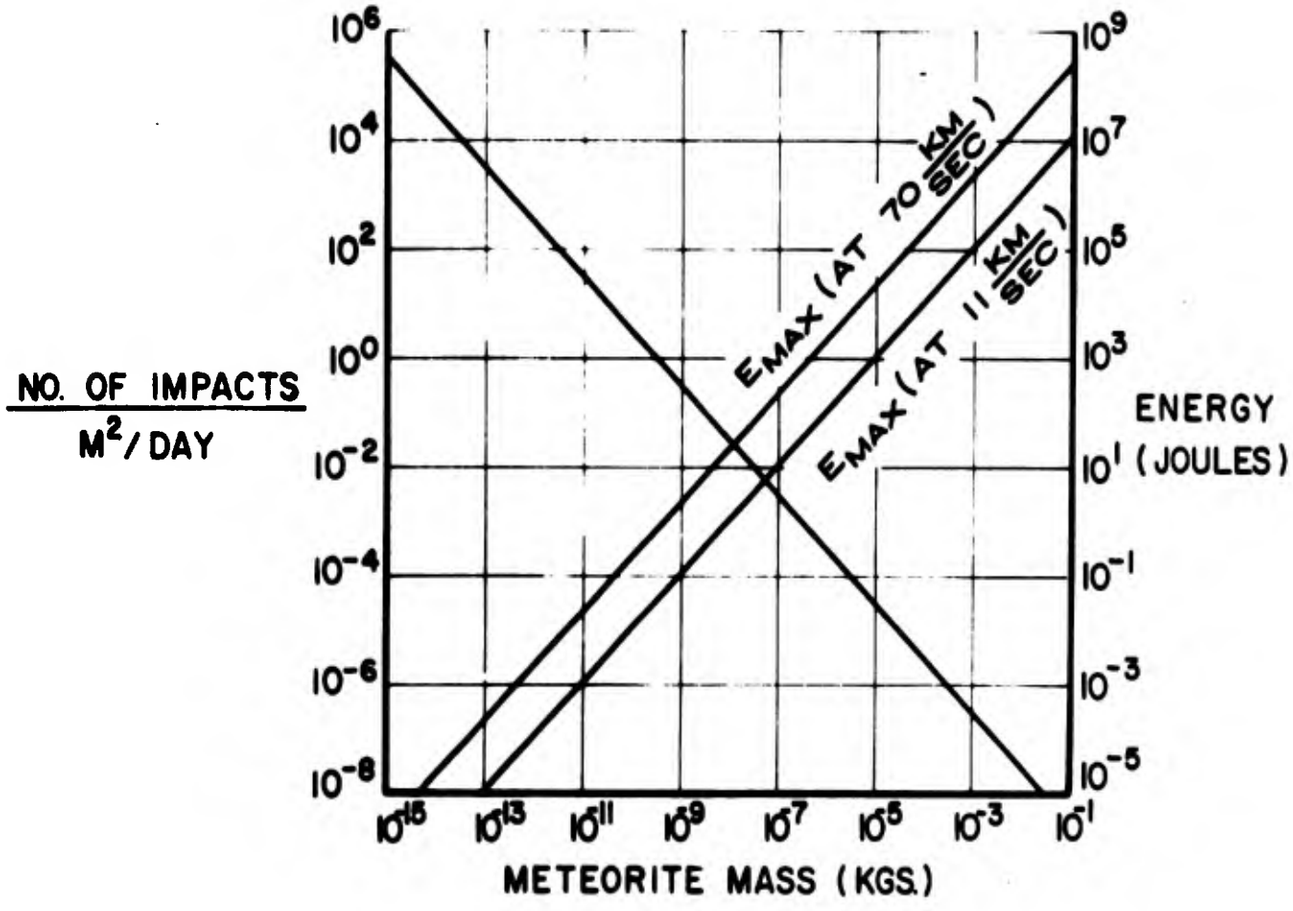

FREQUENCY DISTRIBUTION AND POSSIBLE ENERGY RANGE AS FUNCTIONS OF METEORITE MASS

(AFTER F. C. JONAH: CRITICAL ANALYSIS OF SOLID DEBRIS IN SPACE, IAS PAPER NO. 60-73)

Fig. 1 - Frequency Distribution and Possible Energy Range As Functions of Meteorite Mass (after F. C. Jonah: Critical Analysis of Solid Debris in Space, IAS Paper No. 60-73).

Fig. 2 - Time Sequence of Crater Formation In Aluminum Target

Target Material	= AL - 1100
Pellet Material	= Steel - 1095
Pellet Mass	= 0.18 gm
Pellet Velocity	= 5.01 km/sec.

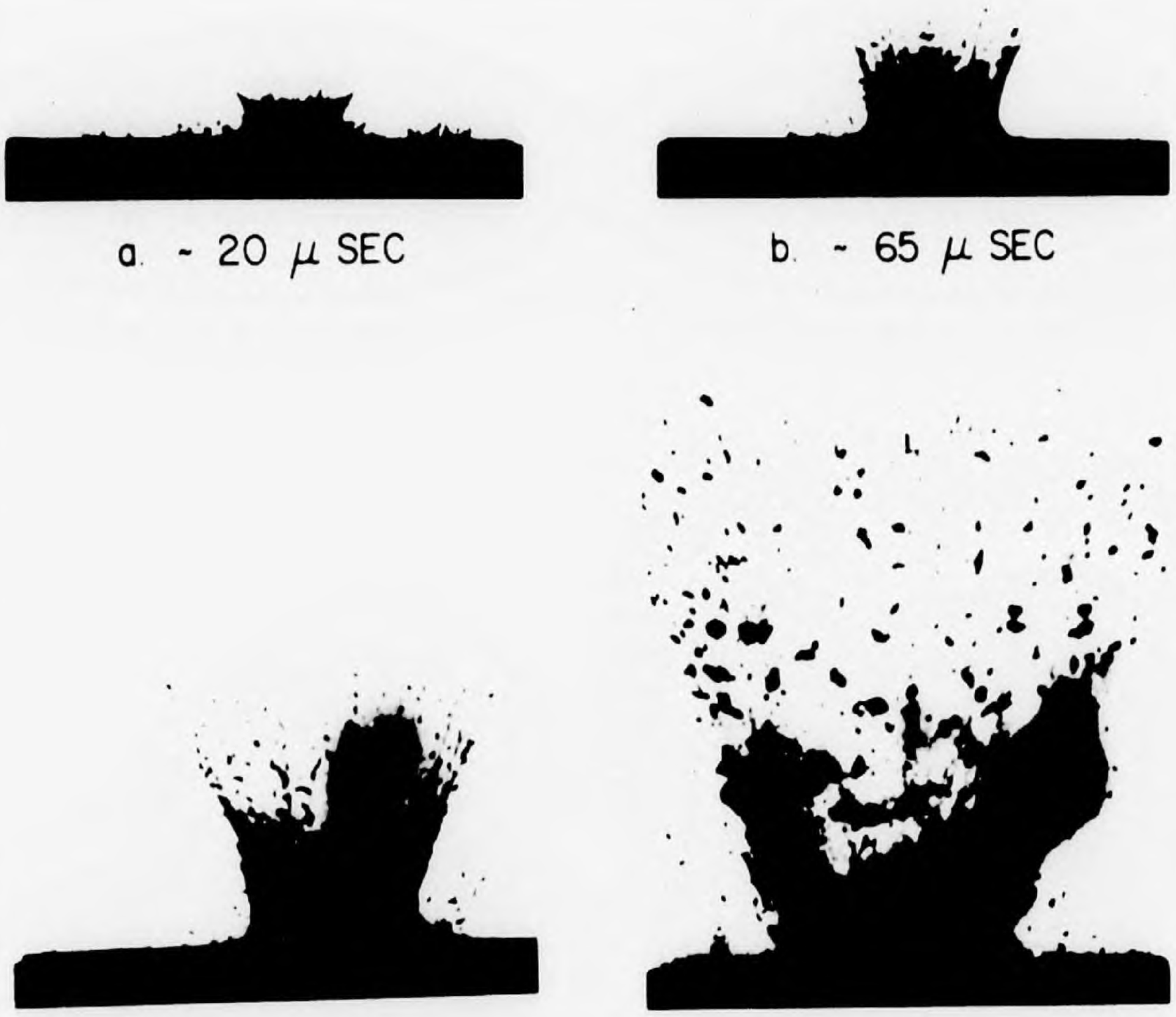

Fig. 3 - Surface Phenomena Associated With Crater Formation In A Lead Target.

Pellet Material = Steel - 1095
Pellet Mass = 2.9 gm
Pellet Velocity = 2.4 km/sec.

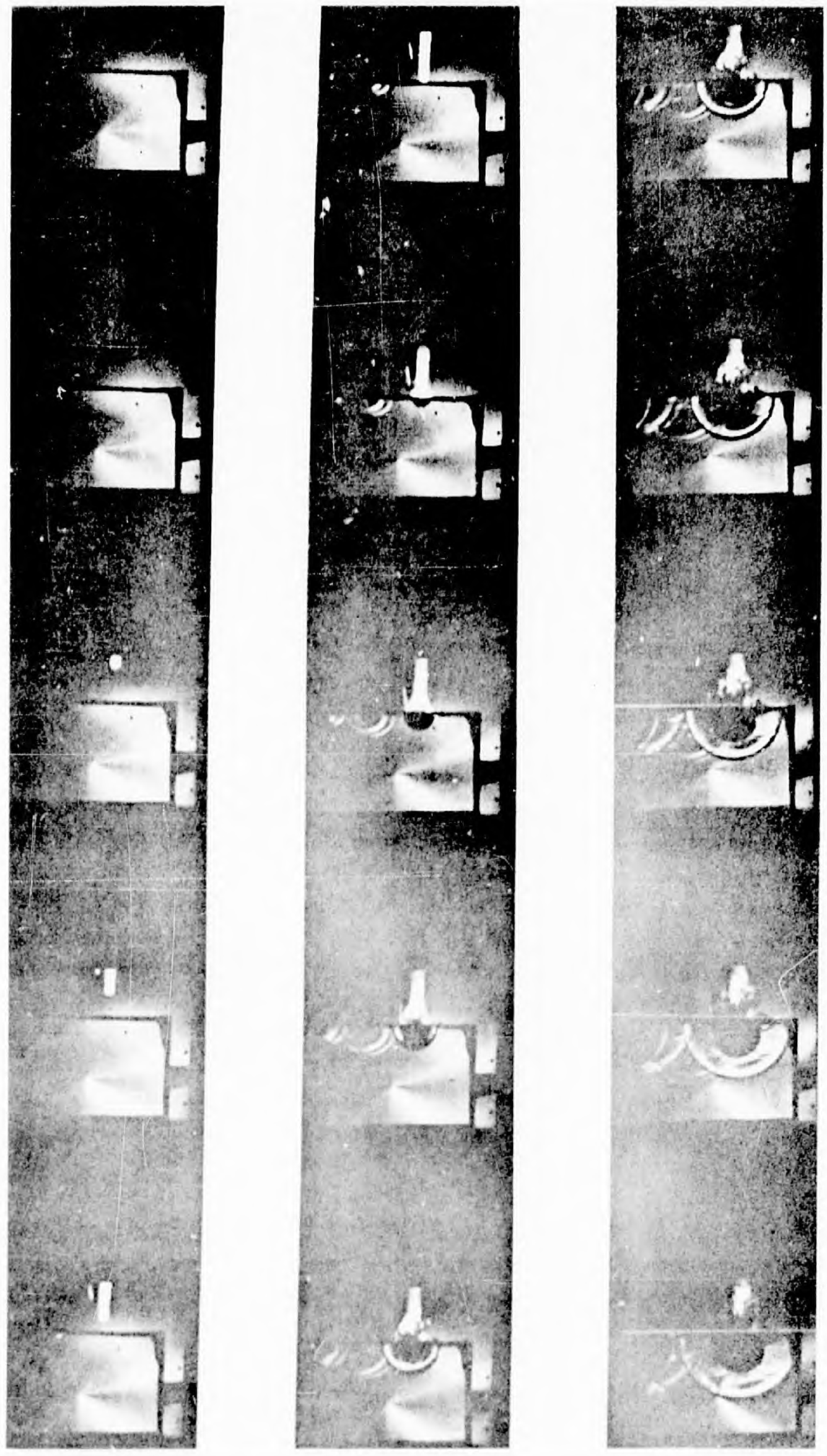

Fig. 4 - Hypervelocity Impact in Lucite

Sequence of high-speed photographs showing a hypervelocity particle striking a lucite target and the subsequent expansion of the crater and propagation of shock waves. Impact velocity = 5.01 km/sec. Time interval between frames = 2 μsec.

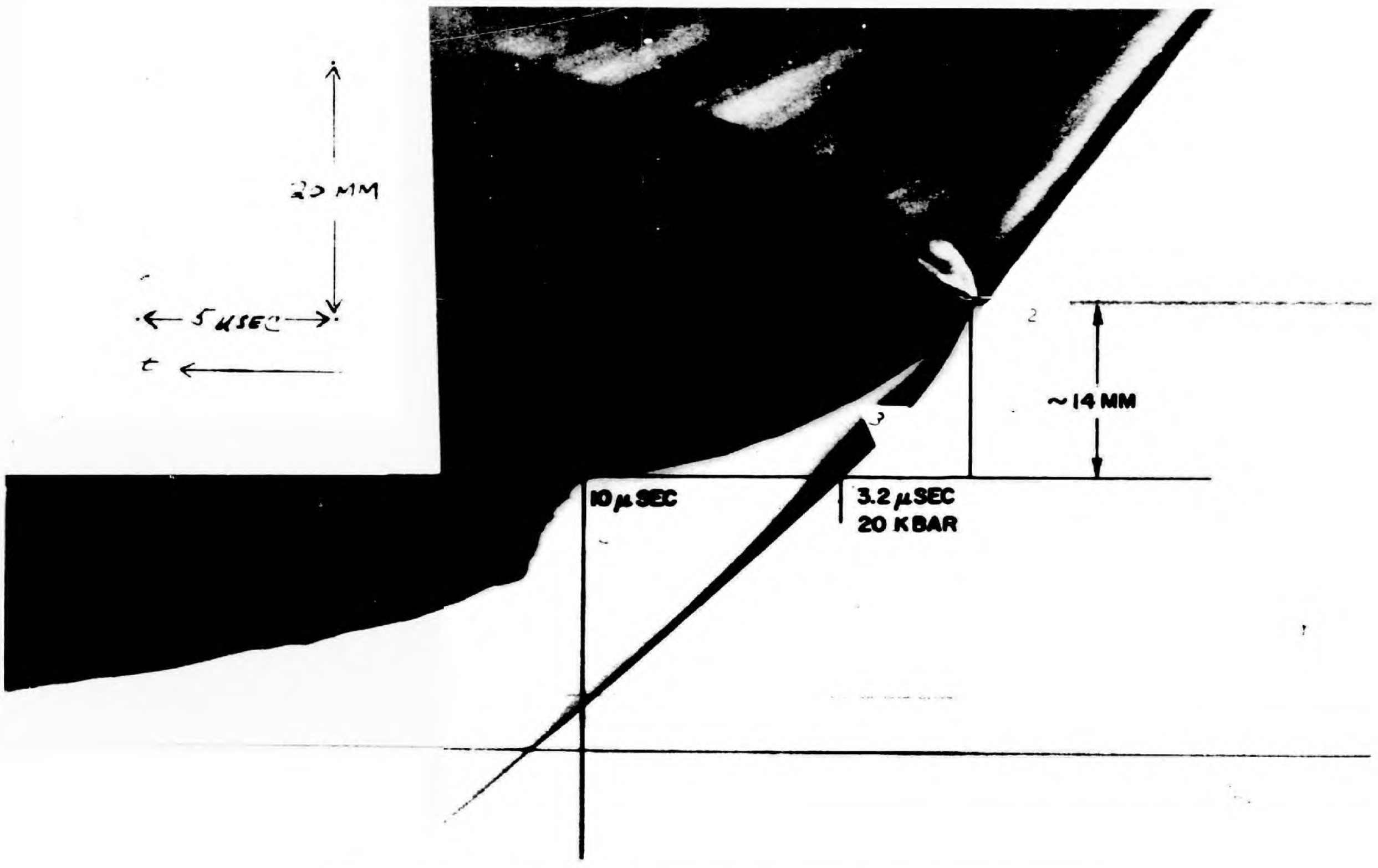

Fig. 5 - Streak Camera Record Of Impact In Lucite Target

1. Steel pellet before striking target. Velocity = 4.6 km/sec.
2. Shock wave in the target.
3. Surface of the expanding crater
4. Envelope of cracks propagating through the target.

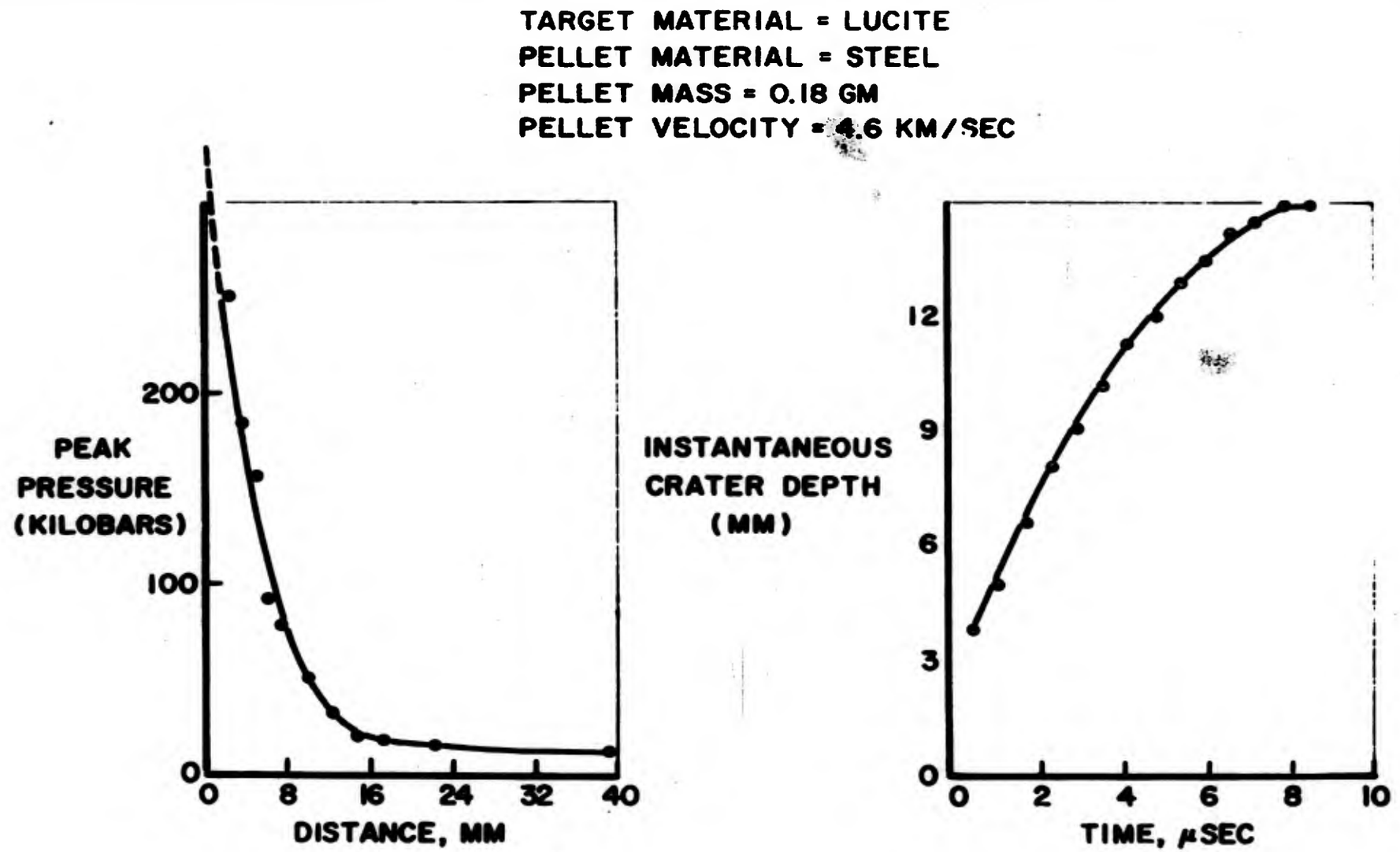

Fig. 6 - Shock Intensity and Rate Of Crater Expansion In A Lucite Target.

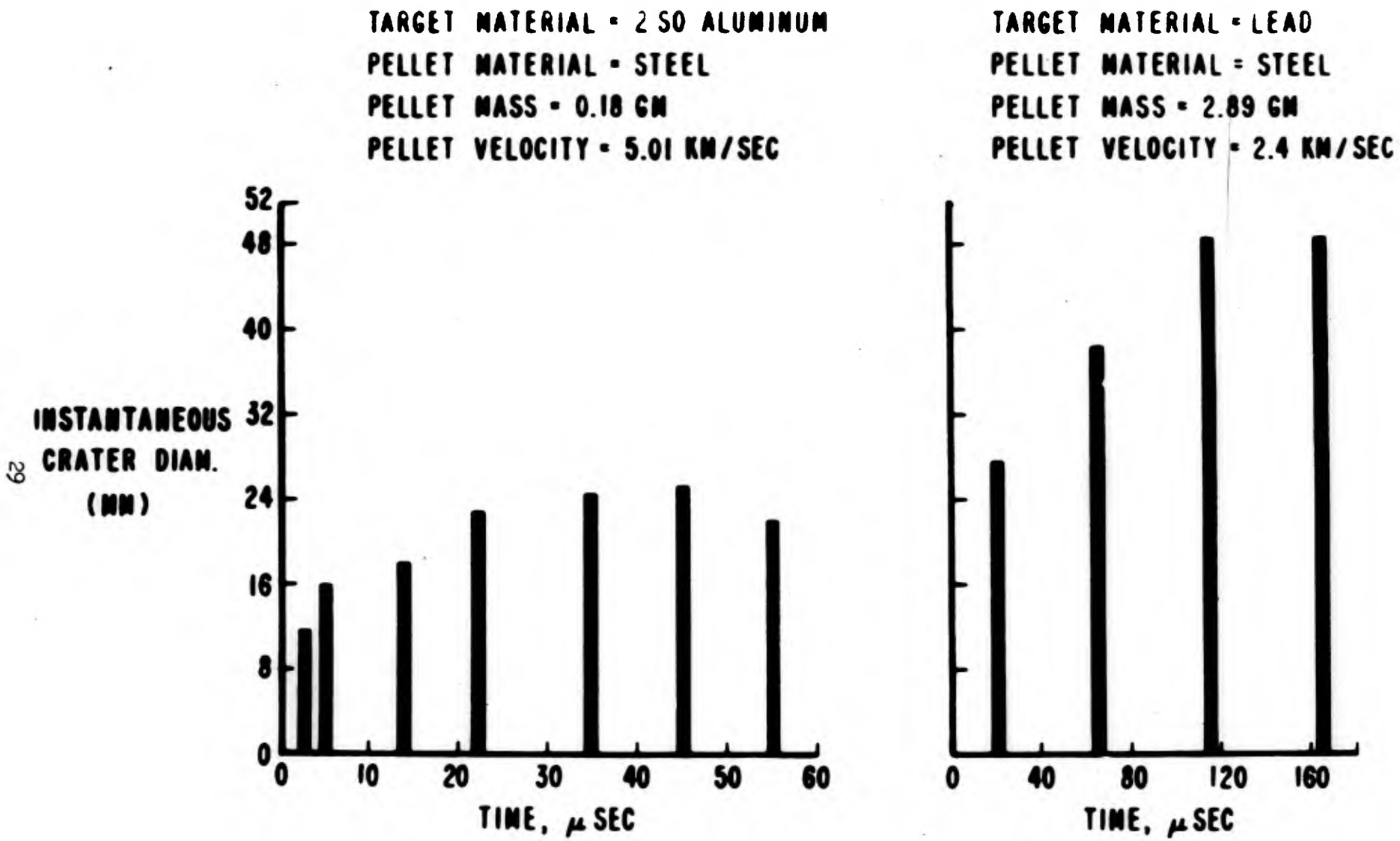

Fig. 7 - Rate Of Crater Expansion In Aluminum and Lead Targets.

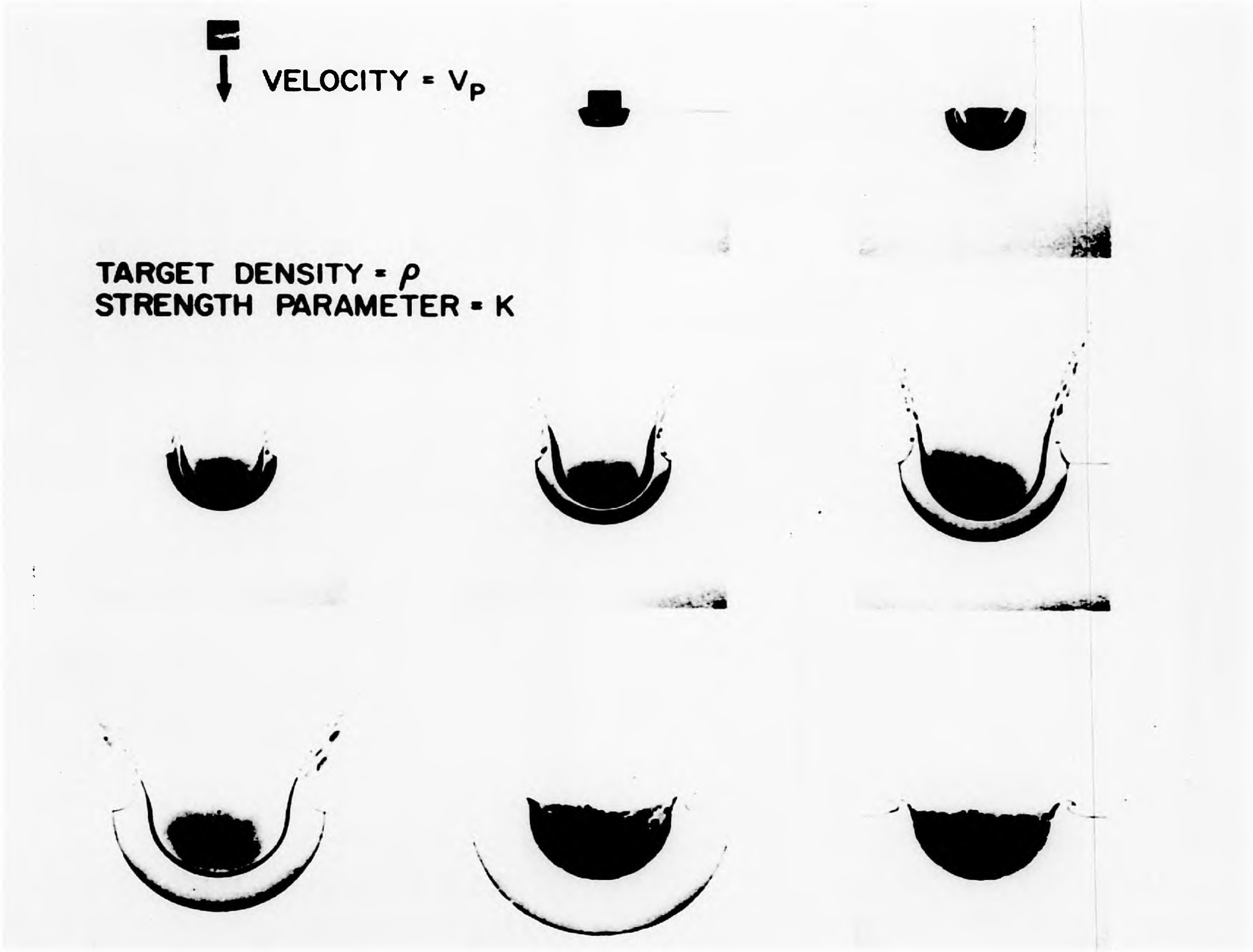

Fig. 8 - Schematic Representation Of Current Concepts Of Crater Formation Under Hypervelocity Impact Conditions.

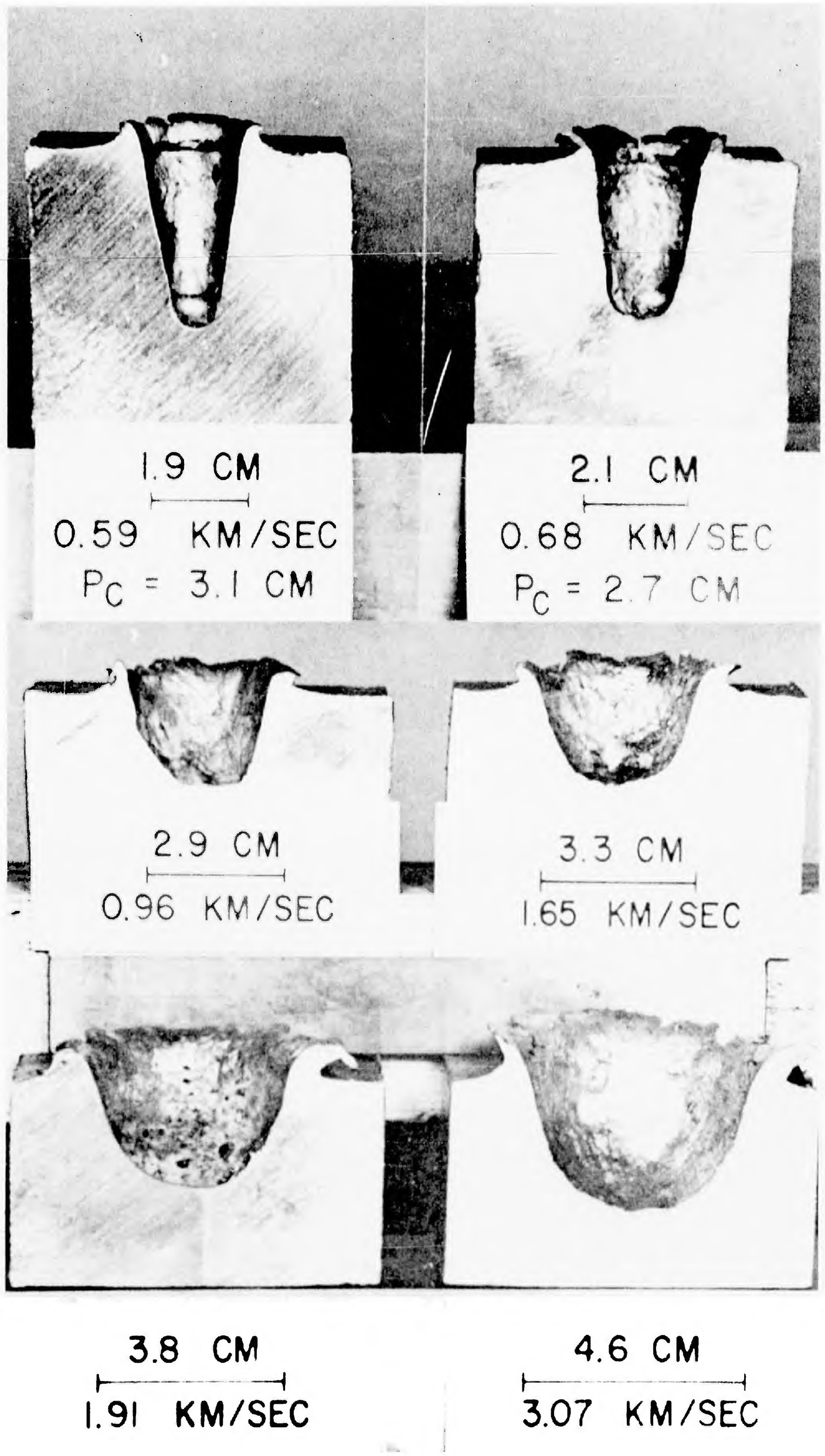

Fig. 9 - Craters Formed In Lead Targets By Steel Projectiles Of Varying Mass and Velocity, Illustrating Change In Crater Shape With Increasing Velocity.

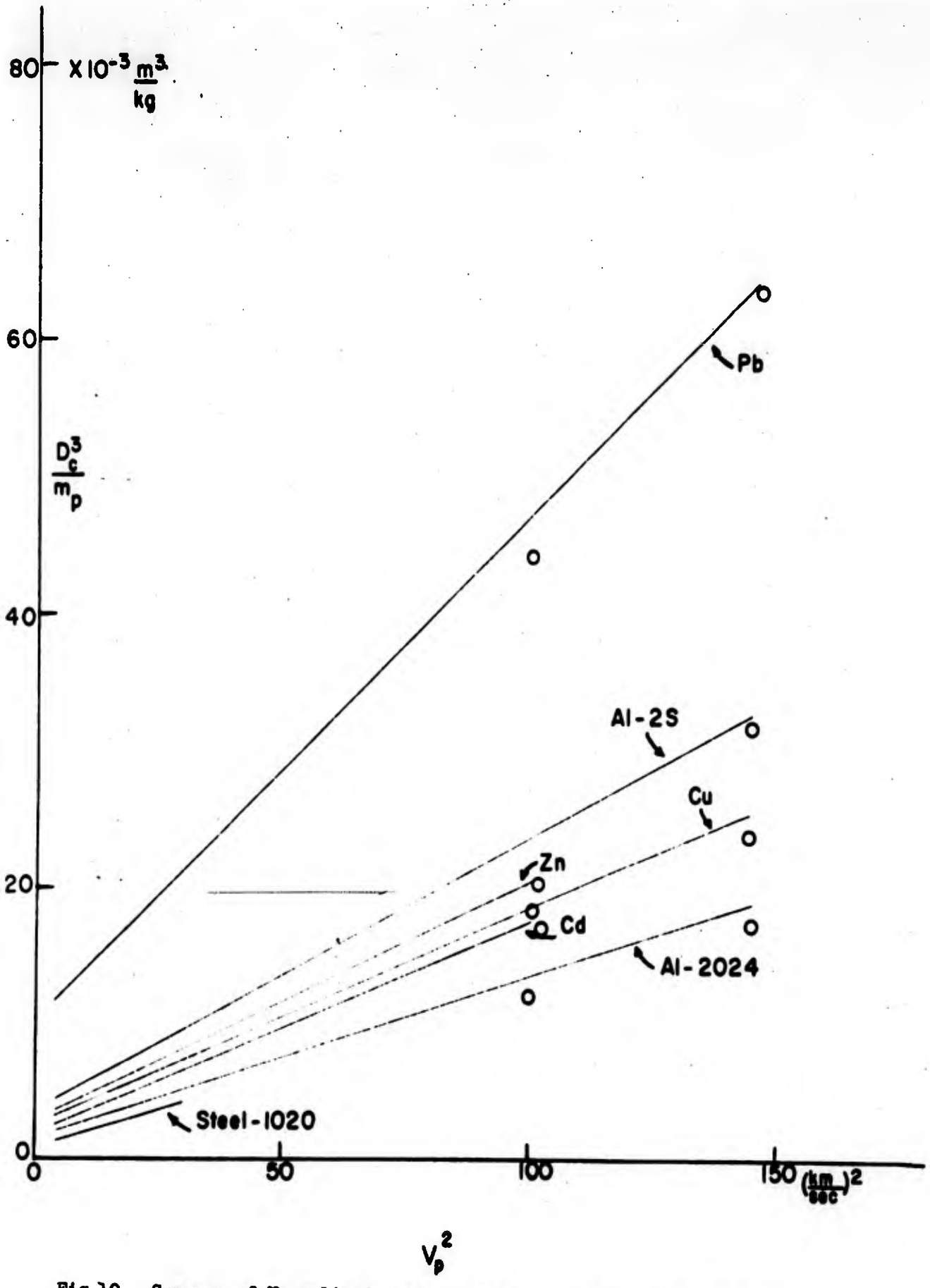

Fig.10 - Summary of Normalized Crater Diameter Data For Seven Metallic Target Materials, At Impact Velocities Up To 12 km/sec. Pellet Material, 1095 Steel. Data Indicate That Crater Volume Is Proportional To Pellet Energy.

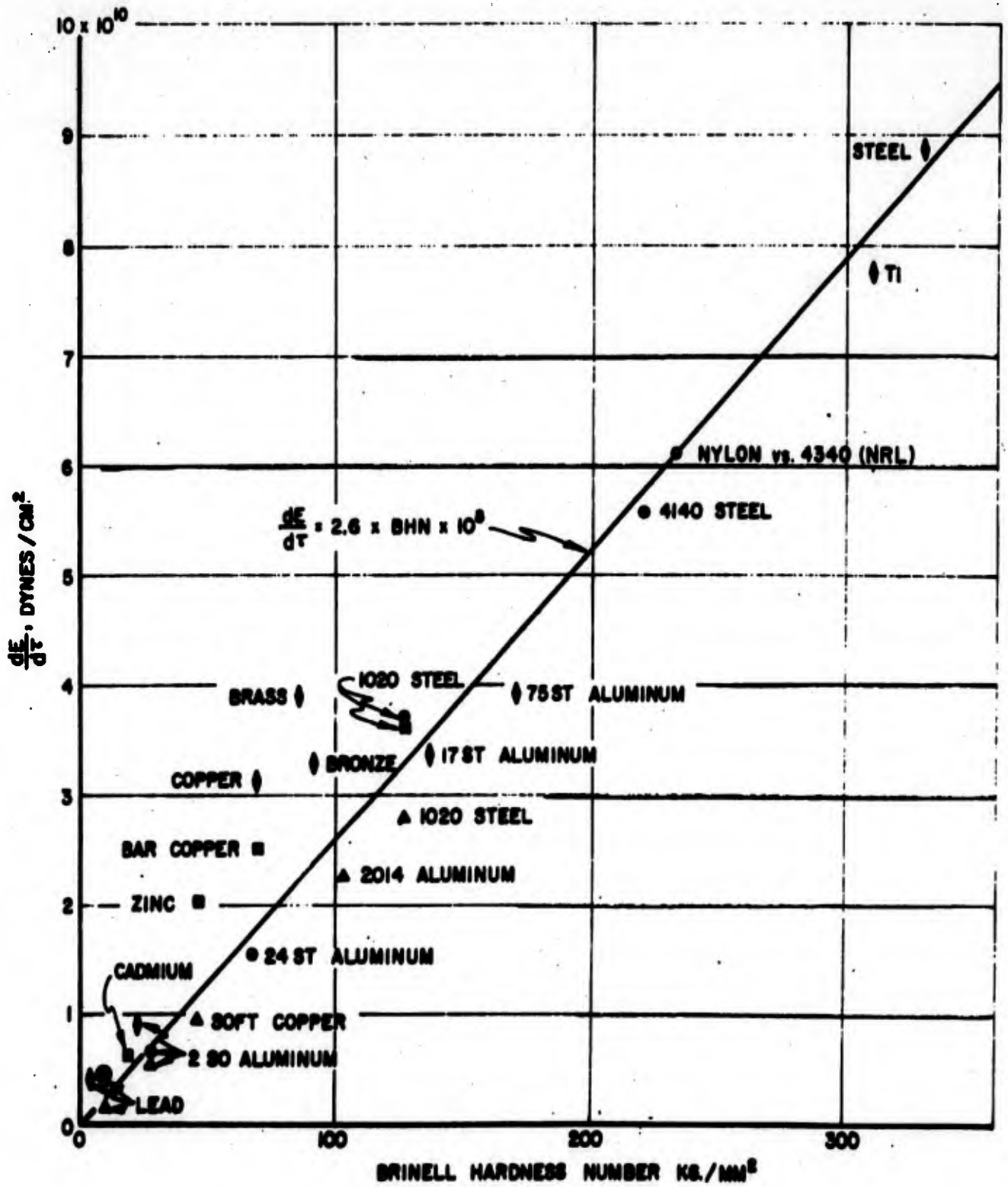

SOURCE:

- ▲ W. ATKINS NRL (TUNGSTEN CARBIDE PELLET)
- ▫ J. KINEKE BRL (STEEL PELLET)
- ○ J. FELDMAN BRL (CONTINUOUS COPPER JET)
- ◊ R. EICHELBERGER CIT (STEEL PELLET)

Fig.11 - Cratering Efficiency as a function of Brinell Hardness Number.

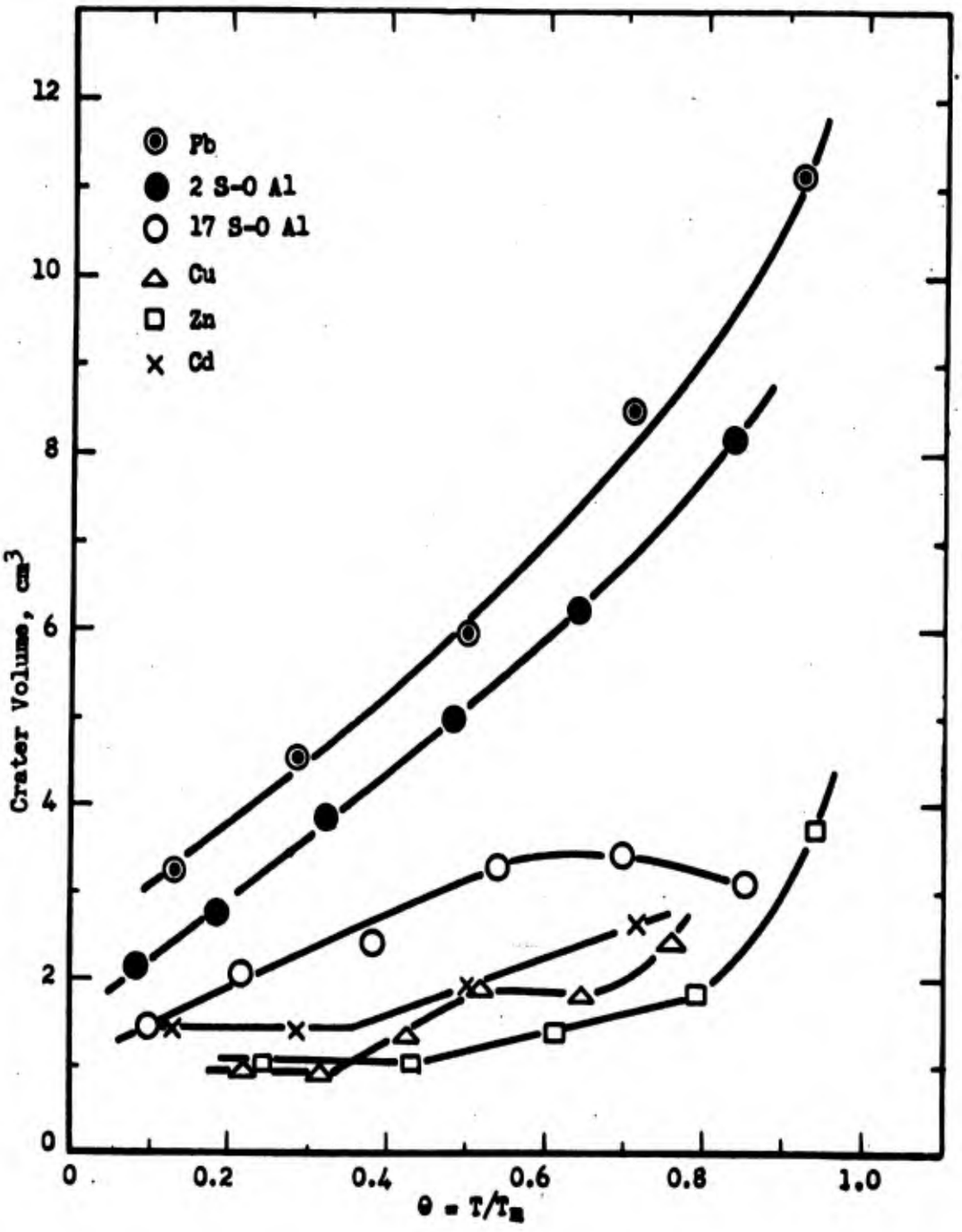

Fig.12 - Effect Of Target Temperature On Crater Volume.

Pellet Material = Steel (1095)
Pellet Mass = 0.18 grams
Pellet Velocity = 5.01 km/sec.

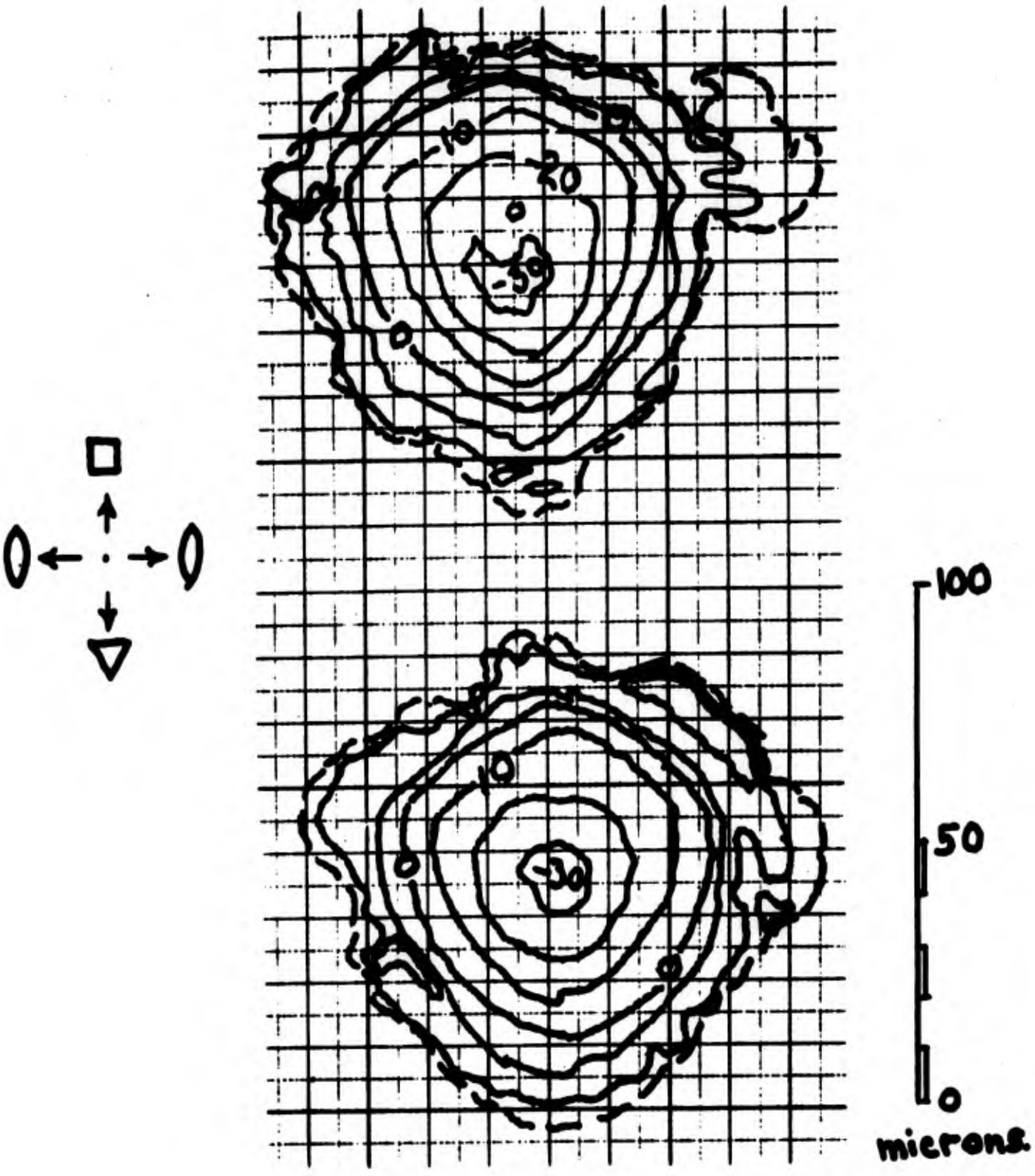

Fig.13 - Micro Craters In Single Crystals..

Contour diagrams of typical hypervelocity craters made by iron particles striking at 10 km/sec.

Single crystal specimens of copper had the (112) face in the plane of the target surface.
Contour interval = 10 microns.

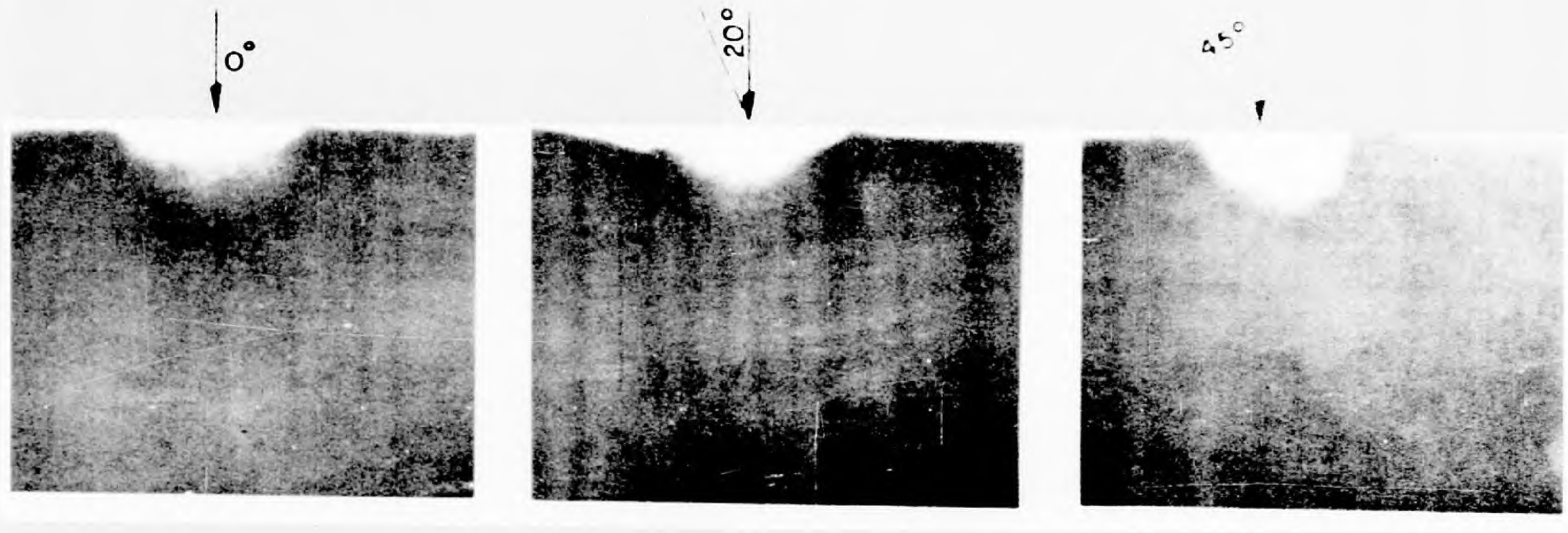

Fig.14 - Crater Formation In Aluminum At Varying Angles Of Attack.
Pellet Material = steel - 1095
Pellet Mass = 0.18 gm.
Pellet Velocity = 5.01 km/sec.
Radiographed 50 μsec after impact.

30°
2.32 KM/SEC

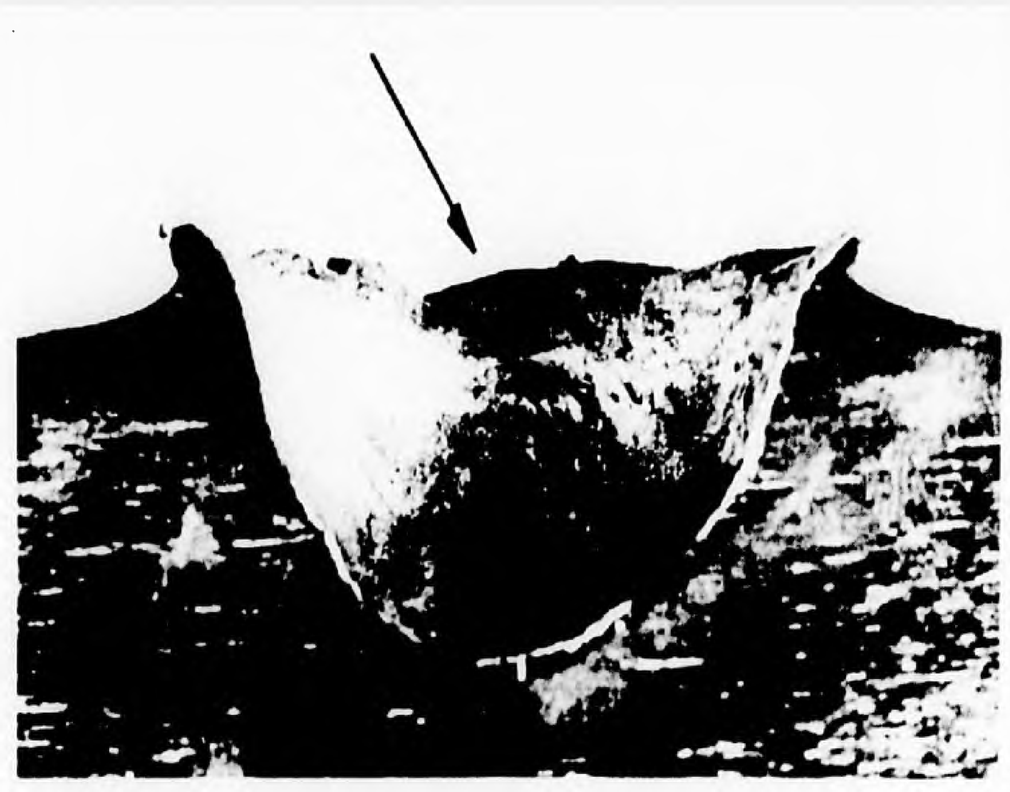

60°
2.32 KM/SEC

60°
3.22 KM/SEC

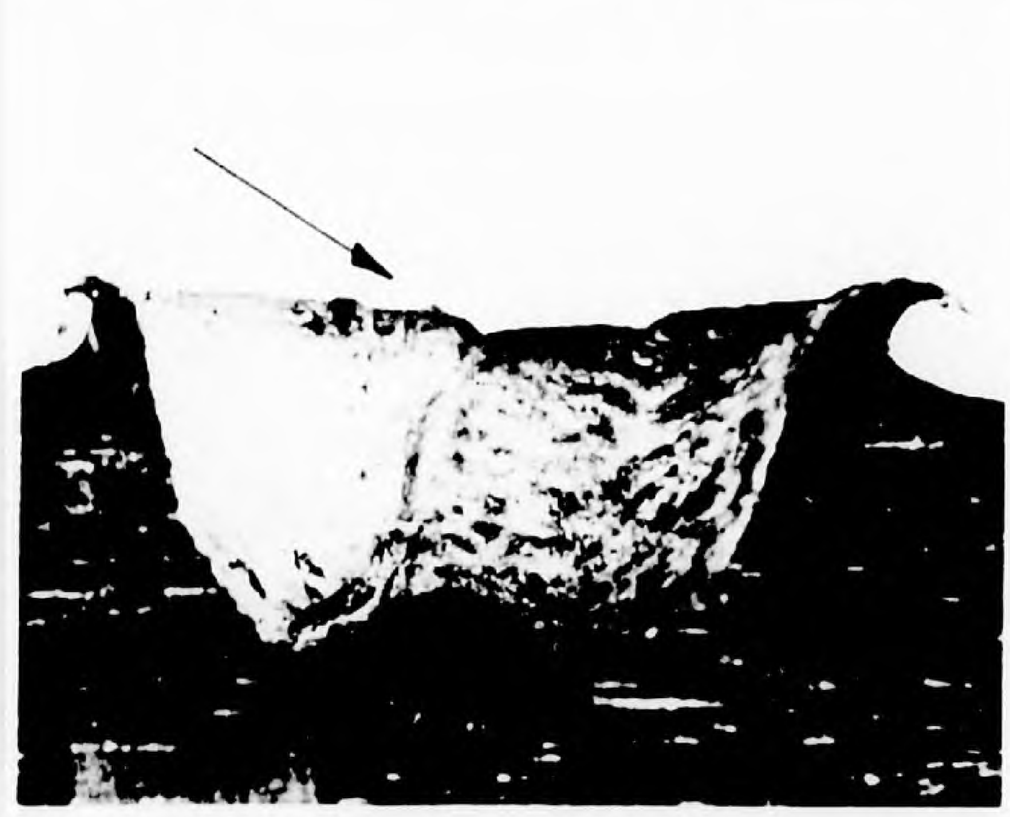

Fig. 15 - Effect Of Angle Of Attack On Hypervelocity Cratering.

Craters formed in lead targets by steel projectiles of constant mass, but varying velocity and angle of incidence; illustrating the interaction between the two variables and the symmetry of craters produced even at large angles of obliquity when impact velocity is sufficiently high.

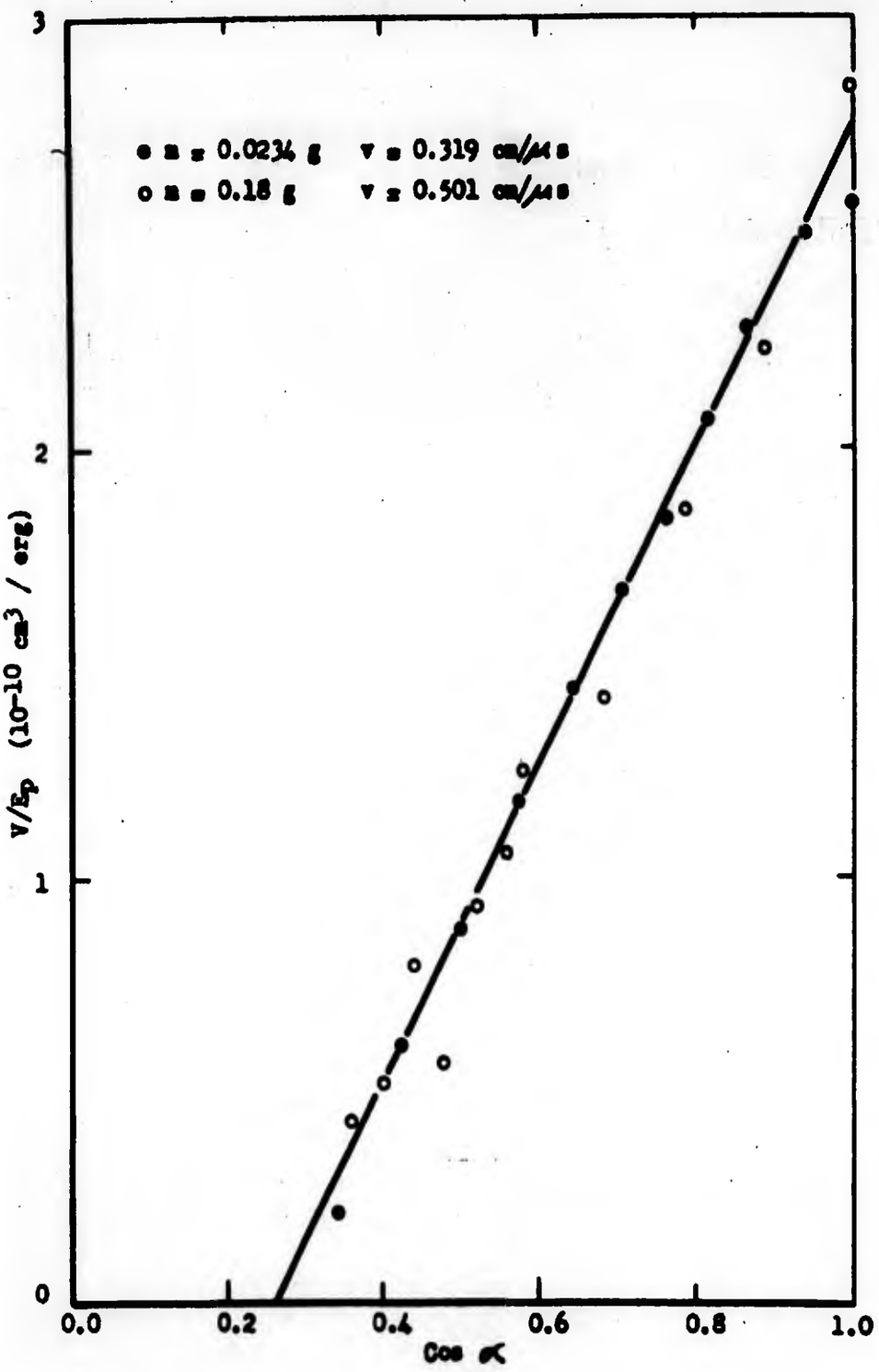

Fig. 16 - Effect Of Angle Of Attack On Cratering Efficiency.

Target Material = Lead
Pellet Material = Steel- 1095

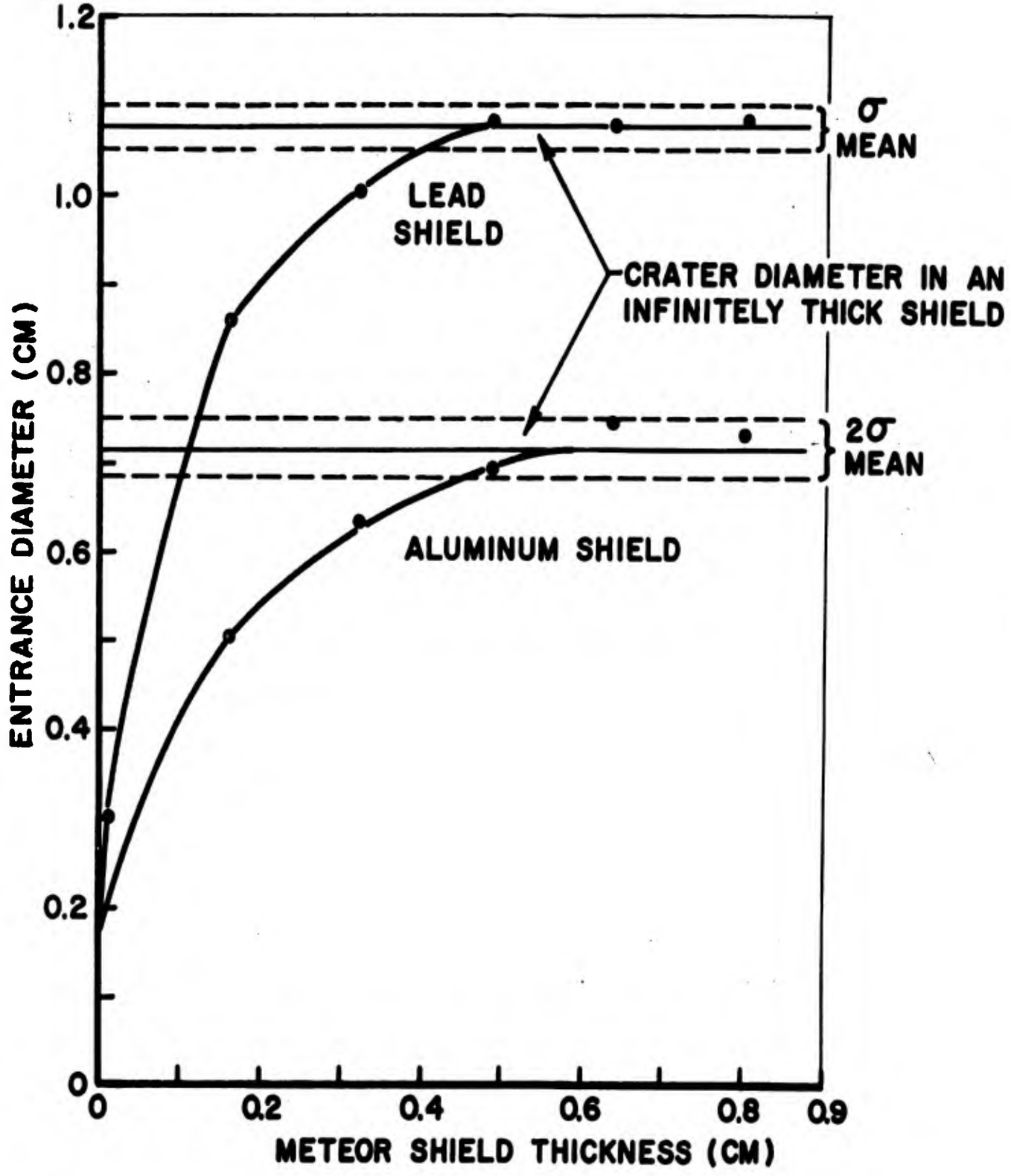

Fig. 17 - Crater Entrance Diameter In Aluminum and Lead Meteor Shields.

Pellet Material = Steel - 1095
Pellet Mass = 0.024 gm.
Pellet Velocity = 3.2 km/sec.

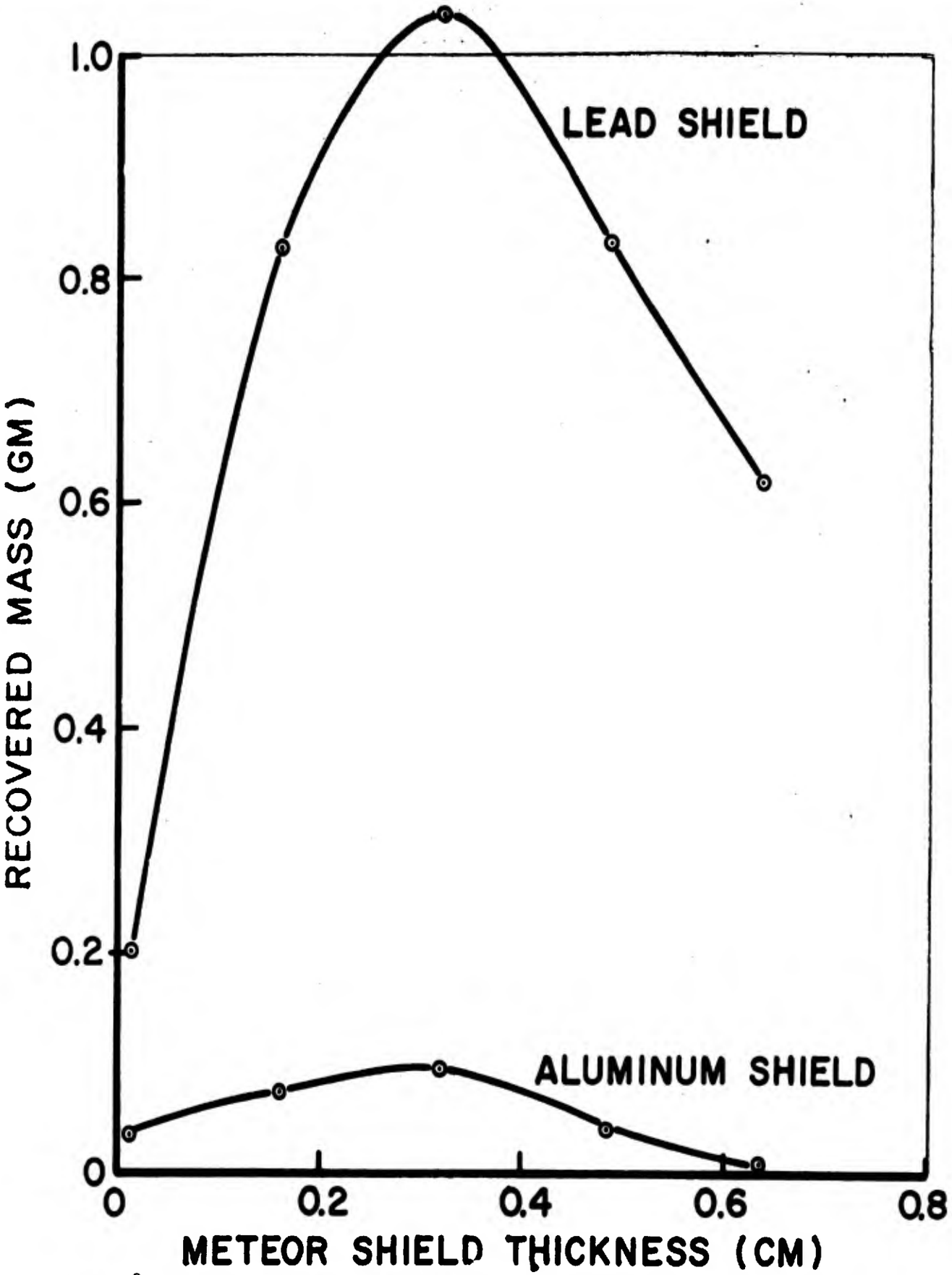

Fig. 18 - Recovered Fragment Mass Behind Aluminum and Lead Meteor Shields.

Pellet Material = Steel - 1095
Pellet Mass = 0.024 gm.
Pellet Velocity = 3.2 km/sec.

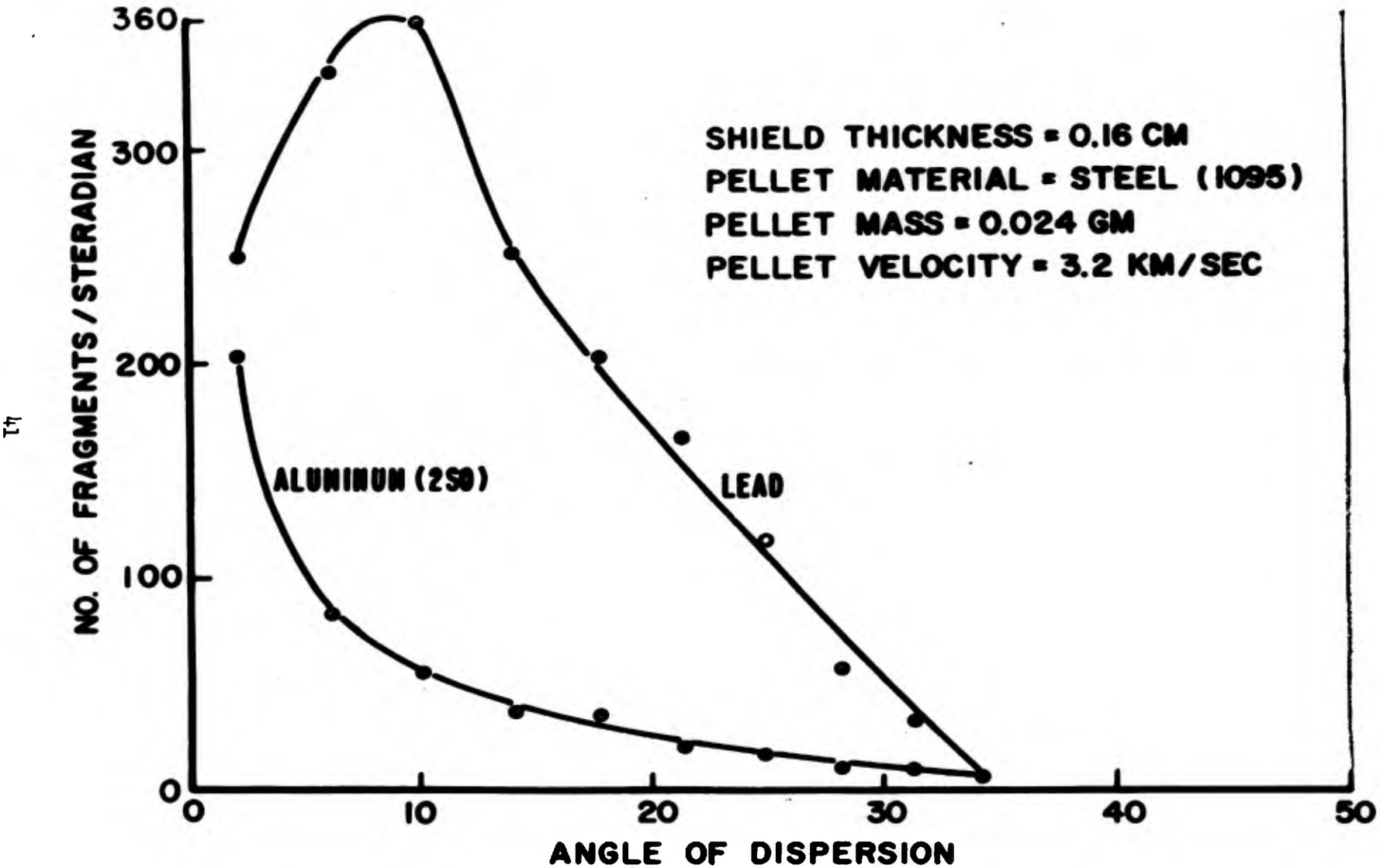

Fig. 19 - Angular Distribution Of Fragments Behind Aluminum and Lead Meteor Shields.

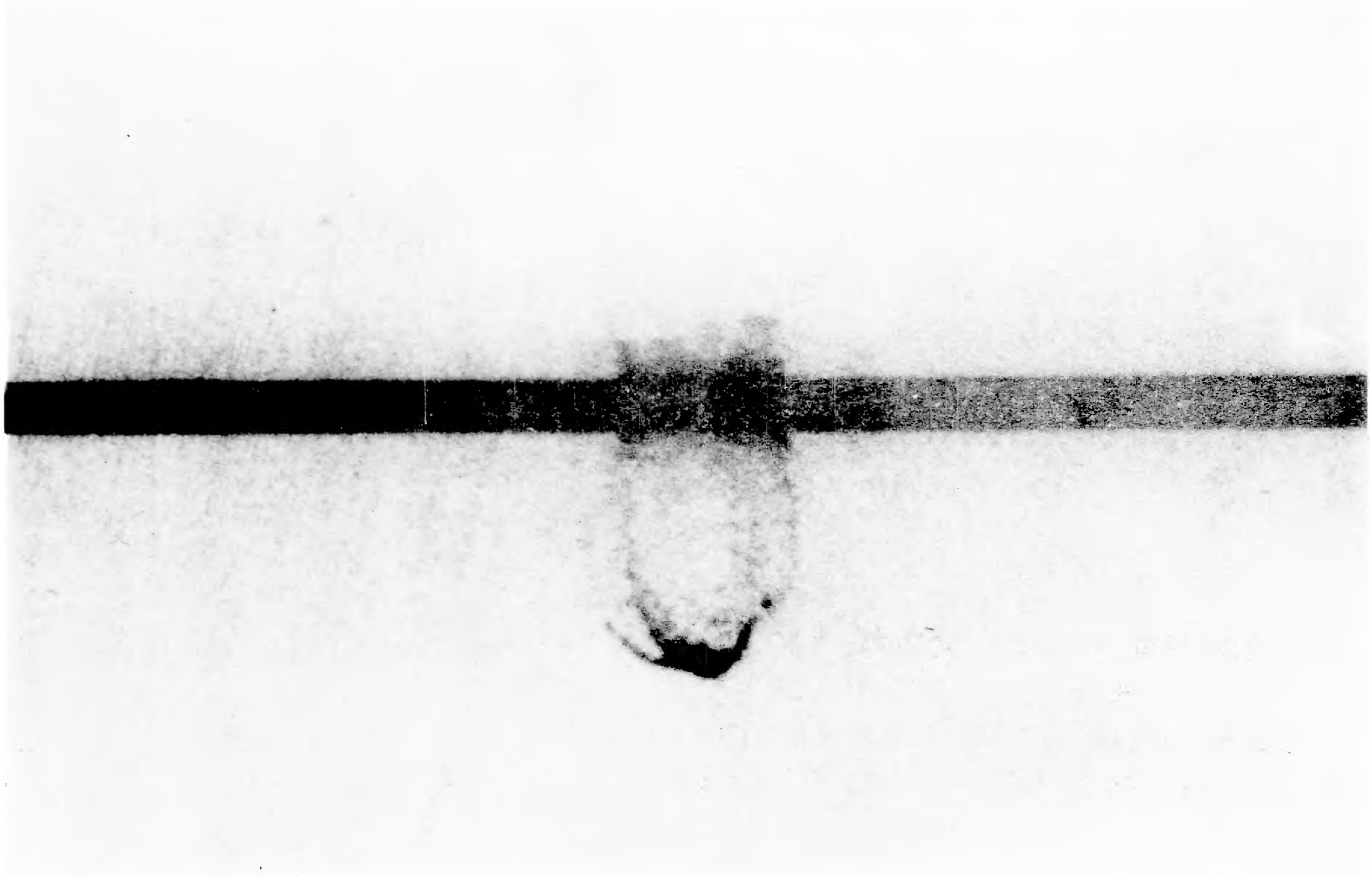

Fig. 20 - Residual Pellet and Spall Pattern 10 μsec After Impact On 0.32 cm Thick Aluminum (2024) Meteor Shield by a 0.18 gm Steel Pellet Striking at 5.01 km/sec.

DISTRIBUTION LIST

No. of Copies	Organization
10	Commander Armed Services Technical Information Agency ATTN: TIPCR Arlington Hall Station Arlington 12, Virginia
2	Director Advanced Research Project Agency ATTN: Col. R.C. Weidler Department of Defense Washington 25, D.C.
1	Director IDA/Weapon Systems Evaluation Group ATTN: R.C. Duff Room 1E880, The Pentagon Washington 25, D.C.
3	Chief of Ordnance ATTN: ORDTB - Bal Sec ORDTU ORDTX - Dr. G.H. Lee Department of the Army Washington 25, D.C.
2	Commanding General Frankford Arsenal ATTN: C.W. Fleischer - Hyperdynamic Section Library Branch, 0270, Bldg 40 Philadelphia 37, Pennsylvania
3	Commanding Officer Picatinny Arsenal ATTN: E.N. Clark F.E. Saxe Technical Library Dover, New Jersey
2	Commanding Officer Watertown Arsenal ATTN: J.P. McDonough Watertown, Massachusetts
1	Commanding General Army Ballistic Missile Agency ATTN: W.D. Murphree - USAOMC Redstone Arsenal, Alabama
5	Commanding General Army Rocket & Guided Missile Agency ATTN: P.E. Mullowney Redstone Arsenal, Alabama
1	Commanding Officer Diamond Ordnance Fuze Laboratories ATTN: Technical Information Office, Branch 012 Washington 25, D.C.
1	Commanding General Ordnance Weapons Command ATTN: ORDOW-TD, Mr. E.H. Quinnell Rock Island, Illinois
1	Commanding Officer Ordnance Technical Intelligence Agency 400 Arlington Boulevard Arlington Hall Station Arlington, Virginia
1	Institute for Cooperative Research Ballistic Analysis Laboratory ATTN: D. Malick 34th and Charles Street Baltimore 18, Maryland
1	Commanding General Engineer Research and Development Laboratories ATTN: A.L. Anderson U.S. Army Fort Belvoir, Virginia
1	Commanding General U.S. Continental Army Command Fort Monroe, Virginia

DISTRIBUTION LIST

No. of Copies	Organization
1	Commandant U.S. Army Air Defense School ATTN: L.B. Lennon Fort Bliss, Texas
1	Army Research Office Arlington Hall Station Arlington, Virginia
4	Chief, Bureau of Naval Weapons ATTN: DIS-33 Missile Ordnance Branch (RMMO) C.V. Young Department of the Navy Washington 25, D.C.
1	Chief of Naval Research, T-3 ATTN: H. Liebowitz Department of the Navy Washington 25, D.C.
2	Commander Naval Ordnance Laboratory ATTN: H.L. Cartel H.M. Sternberg White Oak, Dilver Spring 19 Maryland
1	Commanding Officer U.S. Naval Ordnance Test Station ATTN: J.W. Rogers China Lake, California
2	Director U.S. Naval Research Laboratory ATTN: Mr. W.W. Atkins, Code 130 Washington 25, D.C.
1	Commander U.S. Naval Weapons Laboratory ATTN: J.C. Talley Dahlgren, Virginia
1	Commander Air Force Systems Command ATTN: SCRR Andrews Air Force Base Washington 25, D.C.
4	Commander Air Proving Ground Center ATTN: PGAPI H.L. Davis Lt. W.H. Dittrich - Det. 4, ASD (ASQWR) F.E. Howard - Det. 4, ASD (ASQP) Eglin Air Force Base, Florida
1	Commanding Officer North American Air Defense Command ATTN: J.W. Armstrong Ent Air Force Base Colorado Springs, Colorado
2	Commander Air Force Special Weapons Center ATTN: Capt. C.M. Gillespie Kirtland Air Force Base, New Mexico
2	Commander Aeronautical Research Laboratory ATTN: R.G. Dunn Technical Library Wright-Patterson Air Force Base, Ohio
1	Director U.S. Geological Survey ATTN: H.J. Moore Washington 25, D.C.
1	Library of Congress Technical Information Division ATTN: Bibliography Section Reference Department Washington 25, D.C.

DISTRIBUTION LIST

No. of Copies	Organization
1	Director Pittsburgh Research Center Bureau of Mines ATTN: Chief, Explosives & Physical Sciences Division 4800 Forbes Street Pittsburgh 13, Pennsylvania
1	Director National Aeronautics and Space Administration 1520 H Street, N.W. Washington 25, D.C.
2	Director National Aeronautics and Space Administration ATTN: J.L. Summers Technical Library Ames Research Center Moffett Field, California
2	Director National Aeronautics and Space Administration ATTN: M. Dubin Technical Library Goddard Space Flight Center Washington 25, D.C.
2	Director National Aeronautics and Space Administration ATTN: W.H. Kinard Technical Library Langley Research Center Langley Field, Virginia
2	Director National Aeronautics and Space Administration ATTN: E.H. Davison Technical Library Lewis Research Center Cleveland Airport Cleveland, Ohio
1	Aerojet-General Corporation Ordnance Division ATTN: K.N. Kreyenhagen 11711 S. Woodruff Avenue Downey, California
2	Aerospace Corporation ATTN: D.B. Singer Technical Library P.O. Box 95085 Los Angeles 45, California
1	American Machine & Foundry Company Mechanics Research Division ATTN: L.E. Fugelso 7501 N. Natchez Avenue Niles, Illinois
1	ARO, Inc. ATTN: E.H. Goodman P.O. Box 162 Tullahoma, Tennessee
1	Armour Research Foundation Illinois Institute of Technology Center ATTN: F.J. Zimmerman Chicago 16, Illinois
1	Arthur D. Little, Inc. ATTN: D.B. Lull Acorn Park Cambridge, Massachusetts
2	AVCO Manufacturing Corporation Research and Advanced Development Division ATTN: H.E. Hoercher T. Mix 201 Lowell Street Wilmington, Massachusetts
1	Battelle Memorial Institute ATTN: R.F. Badertscher 505 King Street Columbus, Ohio

DISTRIBUTION LIST

No. of Copies	Organization
1	Bell Telephone Laboratories ATTN: J.A. Lewis Whippany Road Whippany, New Jersey
1	Boeing Airplane Company ATTN: R.M. Elam P.O. Box 3707 Seattle 24, Washington
1	Chance-Vought Corporation Astronautics Division ATTN: F.C. Jonah P.O. Box 5907 Dallas, Texas
1	CONVAIR, A Division of General Dynamics Corporation ATTN: G.D. Hopson Fort Worth 1, Texas
2	CONVAIR - Astronautics A Division of General Dynamics Corporation ATTN: A.H. Jazwinski Technical Library P.O. Box 1128 San Diego 12, California
1	Douglas Aircraft Company ATTN: T.J. Wolinski 300 Ocean Park Boulevard Santa Monica, California
1	Firestone Tire & Rubber Company ATTN: C.M. Cox 1200 Firestone Parkway Akron, Ohio
1	General Dynamics Corporation General Atomic Division ATTN: M.F. Scharff P.O. Box 608 San Diego 12, California
2	General Motors Corporation Defense Systems Division, Box T ATTN: J.W. Gehring Technical Library Santa Barbara, California
1	General Mills, Inc. ATTN: J.E. Upton 2003 East Hennepin Avenue Minneapolis 13, Minnesota
2	General Electric Corporation, MSVD ATTN: Technical Library A.M. Smith 3198 Chestnut Street Philadelphia, Pennsylvania
1	Goodyear Aircraft Corporation ATTN: C.D. Stevens 1210 Massillon Road Akron, Ohio
1	Hayes Aircraft Corporation ATTN: C.M. Askey P.O. Box 2287 Birmingham, Alabama
2	The Martin Company Baltimore Division ATTN: T.D. Reisert Technical Library Baltimore 3, Maryland
1	Minneapolis-Honeywell Regulator Co. ATTN: J.A. Bachman, Jr. Minneapolis 40, Minnesota
1	Northrop Aircraft, Inc. ATTN: E.T. Benedikt 1001 E. Broadway Hawthorne, California
1	Northrop Aircraft, Inc. Nortronics Division ATTN: D.D. Parrish Anaheim, California

DISTRIBUTION LIST

No. of Copies	Organization
1	North American Aviation, Inc. Space & Information Systems Division ATTN: C.N. Scully Downey, California
1	Operations Research, Inc. ATTN: R.B. Parlin 8605 Cameron Street Silver Spring, Maryland
3	Director The RAND Corporation ATTN: J.H. Huth R.L. Bjork Technical Library 1700 Main Street Santa Monica, California
1	Raytheon Company Missile Systems Division ATTN: W.A. Hurd Bedford, Massachusetts
1	Republic Aviation Corporation ATTN: J.F. Pereira Farmingdale, Long Island, New York
1	Space Technology Laboratories ATTN: J.F. Friichtenicht P.O. Box 95001 Los Angeles 45, California
1	United Aircraft Corporation Missiles & Space Systems Group ATTN: E.J.H. Lane Hamilton Standard Division Windsor Locks, Connecticut
1	Utah Research & Development Company ATTN: W.N. Clark 1820 Industrial Road Salt Lake City, Utah
3	Applied Physics Laboratory The Johns Hopkins University 8621 Georgia Avenue Silver Spring, Maryland
1	Brown University Engineering Division ATTN: J.T. Frasier Providence, Rhode Island
1	California Institute of Technology Jet Propulsion Laboratory ATTN: R.E. Reed Pasadena, California
2	Carnegie Institute of Technology Department of Physics ATTN: Professor E.M. Pugh R.W. Watson Pittsburgh 13, Pennsylvania
1	Colorado School of Mines ATTN: J.S. Rinehart Golden, Colorado
1	Denver Research Institute University of Denver ATTN: A. Krill Denver, Colorado
1	Massachusetts Institute of Technology Lincoln Laboratory ATTN: R.E. Slattery P.O. Box 73 Lexington 73, Massachusetts
1	Massachusetts Institute of Technology Aeroelastic & Structures Laboratory ATTN: W. Herrmann 77 Massachusetts Avenue Cambridge 39, Massachusetts
1	Pennsylvania State University ATTN: Professor N. Davids University Park, Pennsylvania
1	University of Utah High Velocity Laboratory ATTN: E.P. Palmer 308 Park Building Salt Lake City 12, Utah

DISTRIBUTION LIST

No. of Copies	Organization
10	Commander British Army Staff British Defence Staff (W) ATTN: Reports Officer 3100 Massachusetts Avenue, N.W. Washington 8, D.C.
4	Defence Research Member Canadian Joint Staff 2450 Massachusetts Avenue, N.W. Washington 8, D.C.
	Of Interest to: CARDE

AD_____ Accession No._____

Ballistic Research Laboratories, APG

EFFECTS OF METEOROID IMPACTS ON SPACE VEHICLES

R. J. Eichelberger, J. W. Gehring

BRL Report No. 1155 December 1961

DA Proj No. 503-04-011, OMSC No. 5010.11.833

UNCLASSIFIED

Hypervelocity impact
Space vehicles -
Vulnerability

The mechanism of crater formation due to hypervelocity impact is described, using a variety of experimental observations and theory as a basis. The currently accepted empirical correlations are also presented. The evidence is considered in the light of the problem of meteoroid impacts upon space vehicles, and such generalized predictions as are possible at the present state of the art are derived.

AD_____ Accession No._____

Ballistic Research Laboratories, APG

EFFECTS OF METEOROID IMPACTS ON SPACE VEHICLES

R. J. Eichelberger, J. W. Gehring

BRL Report No. 1155 December 1961

DA Proj No. 503-04-011, OMSC No. 5010.11.833

UNCLASSIFIED

Hypervelocity impact
Space vehicles -
Vulnerability

The mechanism of crater formation due to hypervelocity impact is described, using a variety of experimental observations and theory as a basis. The currently accepted empirical correlations are also presented. The evidence is considered in the light of the problem of meteoroid impacts upon space vehicles, and such generalized predictions as are possible at the present state of the art are derived.

AD_____ Accession No._____

Ballistic Research Laboratories, APG

R. J. Eichelberger, J. W. Gehring

BRL Report No. 1155 December 1961

DA Proj No. 503-04-011, OMSC No. 5010.11.833

UNCLASSIFIED

Hypervelocity impact
Space vehicles -
Vulnerability

The mechanism of crater formation due to hypervelocity impact is described, using a variety of experimental observations and theory as a basis. The currently accepted empirical correlations are also presented. The evidence is considered in the light of the problem of meteoroid impacts upon space vehicles, and such generalized predictions as are possible at the present state of the art are derived.

AD_____ Accession No._____

Ballistic Research Laboratories, APG

R. J. Eichelberger, J. W. Gehring

BRL Report No. 1155 December 1961

DA Proj No. 503-04-011, OMSC No. 5010.11.833

UNCLASSIFIED

Hypervelocity impact
Space vehicles
Vulnerability

The mechanism of crater formation due to hypervelocity impact is described, using a variety of experimental observations and theory as a basis. The currently accepted empirical correlations are also presented. The evidence is considered in the light of the problem of meteoroid impacts upon space vehicles, and such generalized predictions as are possible at the present state of the art are derived.

AD_____ Accession No._____

Ballistic Research Laboratories, APG

EFFECTS OF METEOROID IMPACTS ON SPACE VEHICLES

R. J. Eichelberger, J. W. Gehring

BRL Report No. 1155 December 1961

DA Proj No. 503-04-011, OMSC No. 5010.11.833

UNCLASSIFIED

Hypervelocity impact
Space vehicles -
Vulnerability

The mechanism of crater formation due to hypervelocity impact is described, using a variety of experimental observations and theory as a basis. The currently accepted empirical correlations are also presented. The evidence is considered in the light of the problem of meteoroid impacts upon space vehicles, and such generalized predictions as are possible at the present state of the art are derived.

AD_____ Accession No._____

Ballistic Research Laboratories, APG

EFFECTS OF METEOROID IMPACTS ON SPACE VEHICLES

R. J. Eichelberger, J. W. Gehring

BRL Report No. 1155 December 1961

DA Proj No. 503-04-011, OMSC No. 5010.11.833

UNCLASSIFIED

Hypervelocity impact
Space vehicles -
Vulnerability

The mechanism of crater formation due to hypervelocity impact is described, using a variety of experimental observations and theory as a basis. The currently accepted empirical correlations are also presented. The evidence is considered in the light of the problem of meteoroid impacts upon space vehicles, and such generalized predictions as are possible at the present state of the art are derived.

AD_____ Accession No._____

Ballistic Research Laboratories, APG

R. J. Eichelberger, J. W. Gehring

BRL Report No. 1155 December 1961

DA Proj No. 503-04-011, OMSC No. 5010.11.833

UNCLASSIFIED

Hypervelocity impact
Space vehicles -
Vulnerability

The mechanism of crater formation due to hypervelocity impact is described, using a variety of experimental observations and theory as a basis. The currently accepted empirical correlations are also presented. The evidence is considered in the light of the problem of meteoroid impacts upon space vehicles, and such generalized predictions as are possible at the present state of the art are derived.

AD_____ Accession No._____

Ballistic Research Laboratories, APG

R. J. Eichelberger, J. W. Gehring

BRL Report No. 1155 December 1961

DA Proj No. 503-04-011, OMSC No. 5010.11.833

UNCLASSIFIED

Hypervelocity impact
Space vehicles
Vulnerability

The mechanism of crater formation due to hypervelocity impact is described, using a variety of experimental observations and theory as a basis. The currently accepted empirical correlations are also presented. The evidence is considered in the light of the problem of meteoroid impacts upon space vehicles, and such generalized predictions as are possible at the present state of the art are derived.

UNCLASSIFIED